

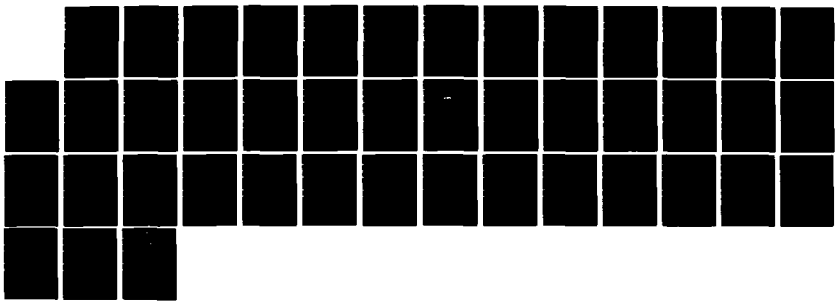
AD-A178 121 BEAM LINE AND ASSOCIATED WORK(U) STANFORD UNIV CA  
W E SPICER ET AL 12 JUL 86 N88814-82-C-8722

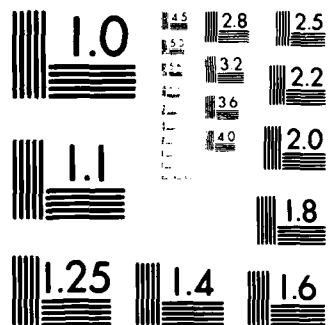
1/1

UNCLASSIFIED

F/G 28/7

NL





MICROCOPY RESOLUTION TEST CHART

NATIONAL BUREAU OF STANDARDS 1963

AD-A170 121

MASTER COPY

FOR REPRODUCTION PURPOSES

12

UNCLASSIFIED

SECURITY CLASSIFICATION OF THIS PAGE (When Data Entered)

| REPORT DOCUMENTATION PAGE  |                       | READ INSTRUCTIONS BEFORE COMPLETING FORM                    |
|--|-----------------------|---|
| REPORT NUMBER  | 2. GOVT ACCESSION NO. | 3. RECIPIENT'S CATALOG NUMBER                               |
|  | N/A                   | N/A   |
| TITLE (and Subtitle)<br><br>Beam Line and Associated Work  |                       | 5. TYPE OF REPORT & PERIOD COVERED<br><br>Final             |
| AUTHOR(s)<br><br>Spicer, W. E.<br>Lindau, I.   |                       | 6. PERFORMING ORG. REPORT NUMBER<br><br>N00014-82-C-0722    |
| PERFORMING ORGANIZATION NAME AND ADDRESS<br><br>Stanford University<br>Stanford, California 94305  |                       | 10. PROGRAM ELEMENT, PROJECT, TASK AREA & WORK UNIT NUMBERS |
| 11. CONTROLLING OFFICE NAME AND ADDRESS<br><br>U. S. Army Research Office<br>Post Office Box 12211<br>Research Triangle Park, NC 27709   |                       | 12. REPORT DATE<br><br>July 12, 1986                        |
| 14. MONITORING AGENCY NAME & ADDRESS(if different from Controlling Office)<br><br>ONR<br>800 N. Quincy Street<br>Arlington, Virginia 22217   |                       | 13. NUMBER OF PAGES<br><br>38                               |
|  |                       | 15. SECURITY CLASS. (of this report)<br><br>Unclassified    |
|  |                       | 15a. DECLASSIFICATION/DOWNGRADING SCHEDULE                  |
| 16. DISTRIBUTION STATEMENT (of this Report)<br><br>Approved for public release; distribution unlimited.  |                       |   |
| 17. DISTRIBUTION STATEMENT (of the abstract entered in Block 20, if different from Report)<br><br>NA   |                       |   |
| 18. SUPPLEMENTARY NOTES<br><br>The view, opinions, and/or findings contained in this report are those of the author(s) and should not be construed as an official Department of the Army position, policy, or decision, unless so designated by other documentation.   |                       |   |
| 19. KEY WORDS (Continue on reverse side if necessary and identify by block number)<br><br>Synchrotron Radiation<br>Undulator Beam Line   |                       |   |
| 20. ABSTRACT (Continue on reverse side if necessary and identify by block number)<br><br>This is the final report of the construction of a beam line at the Stanford Synchrotron Radiation Laboratory. The project was a joint effort between the Department of Defense, the National Science Foundation, the Department of Energy, and the Xerox Corporation. The constructed beam line provides superior photon fluxes in the spectral region 10-1000 eV by using magnetic insertion devices, so-called undulators, on the SPEAR storage ring. The constructed beam line will provide the DOD user community of synchrotron radiation unique spectroscopic capabilities in a variety of studies of atoms, molecules, and solids. |                       |   |

OTIC FILE COPY

**FINAL REPORT**  
**covering the period**  
**July 1, 1982 - September 30, 1985**

**Sponsored by**  
**OFFICE OF NAVAL RESEARCH**

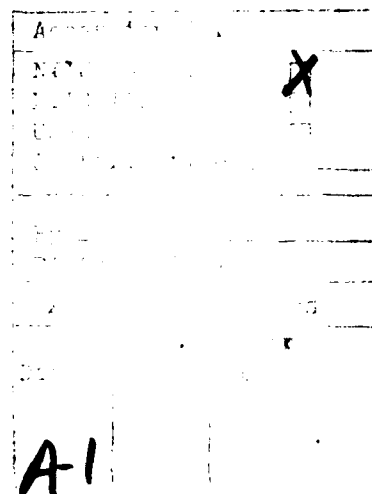
**CONTRACTOR:**                   **The Board of Trustees of the Leland  
Stanford Junior University**

**CONTRACT:**                   **N00014-82-C-0722**

**PRINCIPAL INVESTIGATORS:**   **Prof. W. E. Spicer**  
                                     **Prof. I. Lindau**

**TITLE OF WORK:**              **Beam Line and Associated Work**

**JULY 1986**



BEAM LINE AND ASSOCIATED WORK

P.I.'s: Spicer and Lindau; Contractor N00014-82-C-0722

TABLE OF CONTENTS

|   |    |
|---|----|
| ABSTRACT . . . . .  | 1  |
| 1. INTRODUCTION . . . . .   | 2  |
| 1.1 Overview . . . . .  | 2  |
| 1.2 Background Information . . . . .  | 3  |
| 2. THE BL V MULTI-UNDULATOR . . . . .   | 4  |
| 2.1 Multi-Undulator Design . . . . .  | 4  |
| 2.2 Multi-Undulator Construction . . . . .  | 5  |
| 2.3 Multi-Undulator Controller . . . . .  | 7  |
| 2.4 Multi-Undulator Operational Testing . . . . .   | 7  |
| 3. BEAM TRANSPORT SYSTEM . . . . .  | 8  |
| 4. THE LOCUST MONOCHROMATOR . . . . .   | 9  |
| 4.1 Overview . . . . .  | 9  |
| 4.2 Spectral Ranges and Performance Criteria . . . . .  | 10 |
| 4.3 Configurational Description . . . . .   | 10 |
| 5. REFOCUSING OPTICS AND EXPERIMENTAL AREA . . . . .  | 11 |
| 6. COMPUTER AND CONTROL SYSTEMS . . . . .   | 11 |
| 7. SUMMARY OF OPERATIONAL MILESTONES . . . . .  | 12 |
| 8. LIST OF PUBLISHED PAPERS . . . . .   | 12 |
| 9. APPENDIX: Reprint from paper published in "International Conference on Insulin Devices for Synchrotron Radiation" (R. Tatchyn and I. Lindau, eds.) SPIE 582, 251-267 (1986). | 22 |

ABSTRACT

This is the final report of the construction of a beam line at the Stanford Synchrotron Radiation Laboratory. The project was a joint effort between the Department of Defense, the National Science Foundation, the Department of Energy, and the Xerox Corporation. The constructed beam line provides superior photon fluxes in the spectral region 10-1000 eV by using magnetic insertion devices, so-called undulators, on the SPEAR storage ring. The constructed beam line will provide the DOD user community of synchrotron radiation unique spectroscopic capabilities in a variety of studies of atoms, molecules, and solids.

## 1. INTRODUCTION

This is a final status report on the construction of the DOD funded undulator beam line at the Stanford Synchrotron Radiation Laboratory, Beam Line V. In particular, it highlights the operational success of the new multi-undulator concept which will be of extreme importance for the next generation of synchrotron radiation sources.

Several new aspects of synchrotron radiation beam line design become important when bending magnet sources are replaced by an undulator. The project creating Beam Line V (Wunder) at the Stanford Synchrotron Radiation Laboratory (SSRL) has illucidated and evaluated these aspects for their impact on all the beam line system elements. In this report, we summarize the successful construction and operation of such an undulator beam line. To provide context, we review specific detail on the design and implementation of the beam line. The specific focus for Beam Line V is the spectral range from 10-1000 eV with the design goal to deliver the highest possible power density to the sample in the smallest feasible bandwidth.

### 1.1 Overview

This report summarizes the status of the main beam line elements: the multi-undulator; the beam transport system; the Locust monochromator; the experimental area; and the beam line computer.

The primary system concerns can be partitioned into beam collimation, spectral range, spatial characteristics, and power. In particular, the increased beam power density from an undulator source necessitates active cooling of most elements likely to be hit by the beam. In the case of optical elements, this requirement arises not only because of possible damage but also because distortions of the optics must be minimized to maintain ultimate performance. As a result of our studies, we have shown a new way for

configuring undulators as sources, we have shown the expected improvements to be gained from silicon carbide optics, we have formulated a state of the art second generation soft x-ray monochromator which can handle the high power and deliver high resolution, and we have resolved issues on the best experimental configurations for the development of the next generation of synchrotron radiation sources. The work on Beam Line V thus has direct relevance to beam lines for New Rings and all of our work provides prototype examples. The documentation which we have developed will provide a resource for future projects on undulator-based rings.

### 1.2 Background Information

The project began in 1979 as a bending magnet beam line but shifted to wiggler-undulator technology after the successful operation of a permanent magnet device in SPEAR. In shifting the scope of the plan, the impact of the water cooling requirement on the design of the components in the beam line was greater than initially envisioned.

The collaborative project between Xerox and Stanford motivated the funding from NSF/UIC, DARPA, DOE, and Xerox. The first requirement involved modification of the SPEAR storage ring to free up the physical space for the undulator straight section. This was achieved by replacing the previous four SPEAR designed RF cavities with two of the PEP design. (PEP represented the next generation of storage ring developments at SLAC.) In so doing, this project created the opportunity for the LLNL/UC (Lawrence Livermore National Laboratory/University of California) project at SSRL. The funding required for the construction and installation of these two RF cavities was substantial and caused our beam line development work to be delayed when the initial funding was used to modify the storage ring. In the meantime, we pursued detailed studies both of undulators as sources and of the impact of achieving

the desired performance with the high powers anticipated before embarking on specific designs. These studies led us to the beam line system implementation described here.

## 2. THE BL V MULTI-UNDULATOR

### 2.1 Multi-Undulator Design

Early in the design studies of the beam line, we specified that several undulator periods would be required to span fully the design range of 10-1000 eV. The result of the considerations is the discovery that specific insertions could be sized so that they could be placed close together. Previous to this, considerations for New Rings such as ALS (Advanced Light Source) or the 6 GeV ring had been predicated upon having beam lines with narrow undulator ranges and narrowly defined function. The multi-undulator concept is therefore important for broadly expanding the utility of insertion devices.

The SSRL BL V multi-undulator, shown in Figure 1 with five possible insertion devices (it is now operational with four undulators) has been installed into SPEAR. Its construction and initial operation are described here. Table 1 lists many of the relevant parameters. Figure 1 depicts the five possible insertion devices mounted on individual stainless steel I beams set in the mover structure surrounding the SPEAR beam pipe. The inset shows how the SmCo<sub>5</sub> magnet bars are held. Scanning the undulators can be accomplished in a straightforward manner by varying the magnet jaw gaps of all the undulators simultaneously with the active one positioned over the SPEAR beam pipe. Interchange between the different periods can then be carried out by opening the jaws to full gap and sliding the undulators across the beam pipe within the confines of the SPEAR funnel. An important part of the design is the end coil corrections which were implemented with electromagnets.

The multi-undulator innovation represents a major advance in the art of permanent magnet undulator devices and solves the problem of achieving a wide range while remaining in the undulator regime. We have chosen to implement devices with  $N = 10, 15, 24$  and  $30$  periods in the available  $183$  cm SPEAR straight section corresponding to  $18.3, 12.2, 7.6$  and  $6.1$  cm period lengths.

Table 1 summarizes the parameters characterizing the Multi-undulator for SPEAR operating at  $3$  GeV, a typical dedicated operating condition. For each device, the range of the fundamental will have a low energy cutoff set by the requirement that the magnets have a remanent field of  $0.93$  Tesla and a minimum gap of  $3.0$  cm, and an absolute high energy cutoff set by  $K = 0$ . Table 1 shows the tuning ranges achievable with the multi-undulator based upon power criteria and also characterizes the photon energy and radiated power at  $K$  values of  $3.5, 1.4$ , and  $0.5$  corresponding to the half power and maximum of the fundamental.

## 2.2 Multi-Undulator Construction

The multi-undulator consists of the individual period insertions, the mover frame, and the control electronics. The periods are built up from SmCo5 blocks mounted into keepers which are then attached to the I beams mounted in the mover frame. The mover is constructed to be able to separate the magnet jaws while keeping them parallel to within  $1$  mil of the two meter length. The drive systems allows for a vertical scanning resolution of  $1$  mil. In the original design, everything above the horizontal slide except the magnets was made of stainless or aluminum to minimize the possibility of field distortions. Due to delivery problems, magnetic steel lead screws were substituted in order to achieve this summer's completion. As described below, this substitution does not seem to have led to operational problems.

In the first phototype permanent magnet undulator tested at SSRL, the magnets were epoxied to the keepers. We have developed a scheme for mechanically clamping

the magnets which eliminates the gluing shown in Figure 1. The square cross section magnet bars are beveled on the ends, such that the bars can be clamped into the keeper with a flush mounting design, so that the minimum achievable gap is not compromised. Thus, we can still use the minimum 3 cm gap available with the SPEAR vacuum chamber. The substitution of mechanical clamping for gluing results in substantial reduction of assembly labor and, in addition, permits correction of problems should they develop.

The first phase of the assembly of the insertions upon receipt of the magnets is inspection of the magnets. Examination of the measurements provided by the manufacturer relative to tests made at SSRL showed that remeasuring was not needed. Thus, the magnets were checked for uniformity and for mislabeling with a visualization card and then set on rubber cushioned steel plates for storage. Once a pool of acceptable magnets was designated, the sorting was performed by computer (details can be found in a paper by Youngman and Cox published in the SPIE Proceedings of the International Conference on Insertion Devices for Synchrotron Radiation, edited by R. Tatchyn and I. Lindau, Vol. 582, pp. 91-97). A previous hand sort had taken three weeks, and the computer sort required only several hours of computer time. The physical magnets were then arranged according to the sort and inserted into the keepers using some specially prepared fixturing. The individual keepers were then mounted onto the I beams, putting the upper ones in first and then covering them with a prospective spacer.

Once the I beams were set, the phase was checked with the visualization card and measurements taken using a coil and integrating voltmeter of  $\int B \cdot dl$ . The measurements were taken as a function of gap and determined the corrector coil settings required for the integral to be zero.

### 2.3 Multi-Undulator Controller

The controller development was divided into a phase 1 and a phase 2 and, at this time, only phase 1 has been completed. The design and protocols for phase 2 have been completed and will be implemented during the coming year. In the principal operating mode under phase 2, the SPEAR control room will enable the Beam Line V computer to control the variation of the magnet jaw gap within appropriate limits, and the system will track the end coils so that the beam will not move. In Phase 1, the end coils are actuated from the SPEAR computer while the gap can be actuated from either computer. Because of the load on the SPEAR computer, this updating only occurs a few times per second. This places a major limitation on the functional scan rate of the undulator fundamental. The proper design and implementation of the phase 2 controller is essential for a more convenient functional use of the multi-undulator for experimentation.

### 2.4 Multi-Undulator Operational Testing

The testing of the multi-undulator commenced with the 10 and 15 period devices inserted. The presence of these two devices allowed us to explore all aspects of the device. The testing started from the table of compensation measurements developed during the construction. This was tested against operational criteria for beam stability in SPEAR. Extensive machine physics time has been allocated to these studies, and full compatibility of the multi-undulator concept with stable operation of the storage ring has been established.

The testing had several objectives. The first was to refine the trim coil compensation requirements; the second was to characterize any possible tune resonances which might disrupt the operation of the storage ring; the third was to examine any injection problems the presence of the multi-undulator might create; and the fourth was to explore the limits on horizontal exchange with beam in the machine.

An SSRL position monitor was used to determine orbital motion of the beam as the multi-undulator gap is changed. Starting from an extreme open position, the trim coil current required to maintain the beam position as the gap was closed was determined. These measurements essentially reproduced the previously established table.

The horizontal motion of the beam was found to be 3mm per ampere, so that close control of the trim is required to maintain the orbital tolerances required by many of the beam line experiments.

To date, no significant tune resonances have been found, injection is not disturbed by the presence of the multi-undulator, horizontal interchange can be accomplished without dumping the beam, and it seems feasible to track the trim as the horizontal motion is performed so that the beam position will not be significantly disturbed. Several months of operational experience with all four undulators installed for experimental research programs (10, 15, 24 and 30 periods) have been completed with superb performance of the multi-undulator configuration.

### 3. BEAM TRANSPORT SYSTEM

The beam transport system is the backbone of the beam line and incorporates a number of essential elements for beam forming, control, and diagnostics. A series of masks, stoppers, valves, shutters, and apertures constitute the initial control part of the beam line. The masks serve to protect the valves from the beam power loading and also act as radiation shields. The stoppers are an absolute radiation shield and are designed to absorb the full beam should it accidentally dump down the beam line. The apertures define the useful beam and, in the case of an undulator beam line, also serve to spatially filter stray radiation from upstream bending magnets. This stray source of radiation is a severe problem for position monitor design and for the control of the beam in the vicinity of

the beam in the vicinity of the beam line takeoff. Our original design specification called for two sets of adjustable apertures, one in front of the position monitor and one after.

The beam line has both horizontal and vertical steering, but only the vertical steering is maintained with a feed back system. The SPEAR beam position detector consists of a set of 1 mm electrodes set 1 cm apart in the fringe field of the radiation. This positioning was chosen to accommodate the spatial variation of the undulator beam over the range of operating parameters. The spatial extent of an undulator beam varies enormously, so horizontal position detection, in particular, is difficult. The SPEAR beam is currently 6 mm x 1 mm, so that some horizontal sensing can be accomplished, but this is primarily done with intermittent use of fluorescent screens in the diagnostic sections. The position monitoring and steering is still being evaluated because of overlap of radiation from upstream bending magnets with the undulator radiation. Some further refinements of the beam position monitor may turn out to be desirable but the existing system is fully acceptable.

#### 4. THE LOCUST MONOCHROMATOR

##### 4.1 Overview

In specifying a monochromator for this beam line, we sought an instrument which would match well to the undulator and SPEAR characteristics and which would advance the state of the art. The resulting Locust monochromator implements a constant deviation Vodar geometry Rowland Circle mounting and is descended from the Grasshopper Monochromator. By using closed loop computer control and configurational changes, the design incorporates a number of features that would not be achievable with either the Grasshopper or the Extended Range Grasshopper, ERG, configuration for these optics. The Grasshopper was the first fully UHV monochromator, and the LOCUST is the first to be fully water cooled to enable it

to maintain performance with the powers delivered by an undulator. The incorporation of water cooling consistent with accepted vacuum practice while maintaining the required mechanical and optical tolerances proved to be a major problem and added immensely to the scope of design work required.

#### 4.2 Spectral Ranges and Performance Criteria

Achieving the desired ranges shown in Table 2 was a process of considerable trade off. We describe these ranges as optimized predicated by the choice of grating blaze which is within the accessible range. This categorization is useful because all the gratings can go to zero order. Figure 2 shows the resolution versus photon energy over the ranges for each of the gratings. These are accompanied with some flux numbers based upon a theoretical estimate of the monochromator throughput with 100 ma in the ring. Note the high resolution over the wide operating range if realized will be significantly greater than that available with most currently operating instruments and competitive with the best ever achieved. The beam spot size on the sample with the optics described below should be about 0.6 mm half width at focus.

#### 4.3 Configurational Description

Figure 3 shows the primary configurational elements in the monochromator: the entrance separation chamber; the entrance bellows; the moving chamber; the exit chamber; the air bearing system; the laser interferometer; and the granite reference surface. Figure 4a shows the vacuum chamber, while Figure 4b shows the optical mechanism, and the lower half of the vacuum chamber mounted on the granite base. The moving component of the instrument weighs approximately 1300 Kg, but the drive shaft and stepping motor seen in the lower right of Figure 4b is capable of driving the mechanism through a single resolution step in less than 50 msec and attain a maximum velocity of about 10 mm/sec. Thus, the system can scan its full range in about 1.5 minutes.

## 5. REFOCUSING OPTICS AND EXPERIMENTAL AREA

The refocusing system is built into the monochromator. The refocusing system creates three work areas by providing two beams deflected horizontally at 14 degrees from mirrors 0.5 meters from the exit slit and one vertically at four degrees with a mirror 1.0 meter from the exit slit. The side stations are at 2.25 meters and the end station 3.5 meters from their respective mirrors. Although we would have liked to have moved experimental stations further back, the focusing aberrations substantially increased the size of the beam, so that the apertures of typical electron spectrometers would have been overfilled.

The current design is based on toroidal optics with evolution to conically formed optics planned in the future. The two side stations have a more limited energy range than the end station, but this is offset by the participating research groups being able to maintain experimental chambers in place permanently. The end station port is for general use and has no permanently installed chamber. Provision has been developed, however, for rapidly changing positioning chambers including the SSRL facility chambers available for general users. One of the side stations will be used for the DOD user community. It has beeен funded separately from the DOD University Instrumentation Program and is now fully operational.

## 6. COMPUTER AND CONTROL SYSTEMS

The computer system is an integral part of the beam line formulation. Because of the use of closed loop control for coordinating the monochromator, the computer control system is an integral part of the design. All the basic functions of the monochromator are controllable by the computer. In one of the primary scanning modes, the monochromator and the multi-undulator are scanned simultaneously by the computer.

The primary computer shown in Figure 5 is an evolution of our previous PDP11 CAMAC systems at SSRL using the RSX11M operating system and the XC CAMAC device

driver. In the specific implementation, we have used a PDP 11/73 with 512K bytes of memory, 2 RL 02 disks, and an RD 52 30 M byte winchester. An ethernet system utilizing DECNET connects the beam line computer to the SPEAR control room for operation of the multi-undulator. We have created three operating stations consisting of terminals and CAMAC crates, one for each of the experimental areas. In order to achieve the control response time desired, a secondary slave microprocessor was implemented for the control of the monochromator stepping motors operated in a feedback loop with a laser interferometer. It interacts directly with the interferometer encoder and the motors during a move operation. The other beam line motor actuators are driven directly from CAMAC.

The CAMAC system also provides a general data acquisition system. A specialized monochromator/undulator task using the XC driver has been developed which will work in coordination with any of the data acquisition and control program in use at SSRL, e.g., PRG, EXP, and SPECTRA.

## 7. SUMMARY OF OPERATIONAL MILESTONES

The first undulator radiation was extractd from BL V on October 25, 1984, and the beam line was commissioned with one undulator in Jan.-Feb. 1985. The first scientific program was run in June 1985. The multi-undulator stand with two undulators installed was mounted in September 1985 and used for scientific programs Oct. 1985-Feb. 1986. In March 1986, the multi-undulator configuration was completed with all four undulators and has since been used routinely for scientific experimentation. In the fall of 1986 the beam line will provide both quasi-monochromatic undulator radiation and high resolution radiation via the locust monochromator.

## 8. LIST OF PUBLISHED PAPERS

The technical and scientific aspects of the design/construction of the undulator beam line has been described in a number of publications:

1. R. Z. Bachrach, L. E. Swartz, S. B. Hagstrom, I. Lindau, M. H. Hecht, and W. E. Spicer, Nucl. Instr. and Meth. 208, 105 (1983).
2. M. H. Hecht, R. D. Bringans, I. Lindau, and R. Z. Bachrach, Nucl. Inst. and Meth. 208, 113 (1983).
3. R. Z. Bachrach and I. Lindau in "EXAFS and Near Edge Structure," ed. by A. Bianconi, L. Inoccia, and S. Stipcich, Springer-Verlag, N.Y., 1983, p. 415.
4. R. Z. Bachrach, R. D. Bringans, N. Hower, I. Lindau, B. B. Pate, P. Pianetta, R. Tatchyn, and L. E. Swartz, Proc. SPIE 447, 10 (1984).
5. R. Z. Bachrach, R. D. Bringans, N. Hower, I. Lindau, B. B. Pate, P. Pianetta, L. E. Swartz, and R. Tatchyn, Nucl. Instr. and Meth. 222, 70 (1984).
6. R. Z. Bachrach, S. B. Hagstrom, I. Lindau and W. E. Spicer, Annals of the Israel Physical Society 6, 602 (1983).
7. R. Z. Bachrach, R. D. Bringans, B. B. Pate and R. G. Carr, in "International Conference on Insertion Devices for Synchrotron Sources" (R. Tatchyn and I. Lindau, eds.), Proc. SPIE 582, 251 (1986), enclosed as an Appendix.

Some of the first scientific results based on research programs using the undulator beam line has also appeared:

8. W. Eberhardt, E. W. Plummer, C. T. Chem, R. Carr and W. K. Ford, in "Proceedings of the International Conference on X-Ray and VUV Synchrotron Radiation Instrumentation" (G. S. Brown and I. Lindau, eds.), Nucl. Instr. and Meth. 246, 825 (1986).
9. R. Tatchyn, P. L. Csonka, E. Källne, A. Toor, C. Gillespie, I. Lindau and A. Fuller, in "International Conference on Insertion Devices for Synchrotron Sources" (R. Tatchyn and I. Lindau, eds.), Proc. SPIE 582 291 (1986).

## TABLES

1. Xerox/Stanford SSRL BLV Multi-Undulator Parameters.
2. Locust Monochromator Parameters.

## FIGURES

Fig. 1: Pictorial of the Xerox/Stanford SSRL BL V multi-undulator. The five possible insertions mounted on stainless steel I beams are shown installed in the mover assembly surrounding the SPEAR beam pipe. The inset shows how the CMC05 magnet bars are mounted.

Fig. 2: Estimated energy resolution versus photon energy for each of the gratings. The inset numbers give estimated fluxes at the sample for SPEAR running 100 ma at 3 GeV.

Fig. 3: Schematic side view of the Locust Monochromator showing the major assemblies. The details are given in the text. The exit chamber contains the exit slit and the refocusing mirrors.

Fig. 4: Perspective view of the monochromator moving chamber assembly depicted in Figure 3. (a) The vacuum chamber, and (b) the main optical mechanism with the vacuum envelope removed.

Fig. 5: Schematic of the computer system that will control the monochromator and multi-undulator and will support the three experimental stations. Each experimental station has a terminal and CAMAC crate.

TABLE I  
Xerox/Stanford SSRL BLV Multi-Undulator Parameters

|                            |      | Length: 183 cm                        | Miniumum Gap: 3cm                     |                                       |
|----------------------------|------|---------------------------------------|---------------------------------------|---------------------------------------|
|                            |      | SPEAR: 3.0 GeV                        | 100ma                                 |                                       |
| Number of periods          |      | 10                                    | 15                                    | 24                                    |
| Period Length- $\lambda$   | (cm) | 18.3                                  | 12.2                                  | 7.6                                   |
| Magnet Block Size          | (cm) | $\lambda/8 \times \lambda/8 \times 8$ | $\lambda/8 \times \lambda/8 \times 7$ | $\lambda/4 \times \lambda/4 \times 6$ |
| Tuning Range*              | (eV) | 16-417                                | 84-622                                | 360-1020                              |
| K maximum (3 cm gap)       |      | 9.0                                   | 4.6                                   | 2.6                                   |
|                            |      | <u>eV, watts</u>                      | <u>eV, watts</u>                      | <u>eV, watts</u>                      |
| $E_1, P_{tot}$ (max K)     |      | 11.3, 289.4                           | 59.8, 173.2                           | 260.7, 136.3                          |
| $E_1, P_{tot}$ ( $K=3.5$ ) |      | 65.8, 56.6                            | 99.0, 98.5                            | --                                    |
| $E_1, P_{tot}$ ( $K=1.4$ ) |      | 237.5, 7.3                            | 356.3, 16.4                           | 570.0, 42.0                           |
| $E_1, P_{tot}$ ( $K=0.5$ ) |      | 417.0, 0.9                            | 621.6, 2.0                            | 993.4, 5.0                            |
| $E_1, P_{tot}$ ( $K=0.0$ ) |      | 467                                   | 700.8                                 | 1120.6                                |
|                            |      |                                       |                                       | <u>eV, watts</u>                      |
|                            |      |                                       |                                       | 616.5, 82.3                           |
|                            |      |                                       |                                       | --                                    |
|                            |      |                                       |                                       | --                                    |
|                            |      |                                       |                                       | 1245.0, 8.0                           |
|                            |      |                                       |                                       | 1401.6                                |

\* The lower limit of this tuning range is set by the beam line power limit. With suitable power filtering, the maximum K range can be reached. Note that if the storage ring energy is reduced these number scale by the square of the energy.

**TABLE 2**  
**Locust Monochromator Parameters**

Operating Range: 10-1000 eV

100 Watts Input Power

Silicon Carbide Optics

Water Cooled Optics

Laser Interferometer Encoding

Fully Computer Controlled

| Grating Angle             | 2°               | 4°              | 10°             | 20°             |
|---------------------------|------------------|-----------------|-----------------|-----------------|
| Grating Radius (mm)       | 9355             | 4817            | 1986            | 1037            |
| Grating Blank (lwxwxd-mm) | 100x40x30        | 80x40x30        | 60x40x30        | 60x40x30        |
| grooves/mm                | 1200             | 1200            | 600             | 600             |
| Resolution (A)            | 0.0126           | 0.0242          | 0.0593          | 0.1136          |
| S <sub>1</sub> G (mm)     | 3265             | 3360            | 3448            | 3547            |
| Linear Travel (mm)        | 820              | 800             | 400             | 150             |
| Angular Travel            | 5°               | 12°             | 18°             | 13°             |
| Blaze angle               | 1.3°             | 2.0°            | - -*            | - -*            |
| Blaze Energy (eV)         | 600              | 210             | 70*             | 20*             |
| Resolution at Blaze (eV)  | 0.37             | 0.086           | 0.023           | 0.0036          |
| Optimized Range (eV)      | 1500 - 250       | 450 - 90        | 150 - 30        | 50 - 10         |
| Mechanical Range (eV)     | zero order - 220 | zero order - 60 | zero order - 27 | zero order - 10 |

\* These are laminar cylindrical gratings which are not blazed

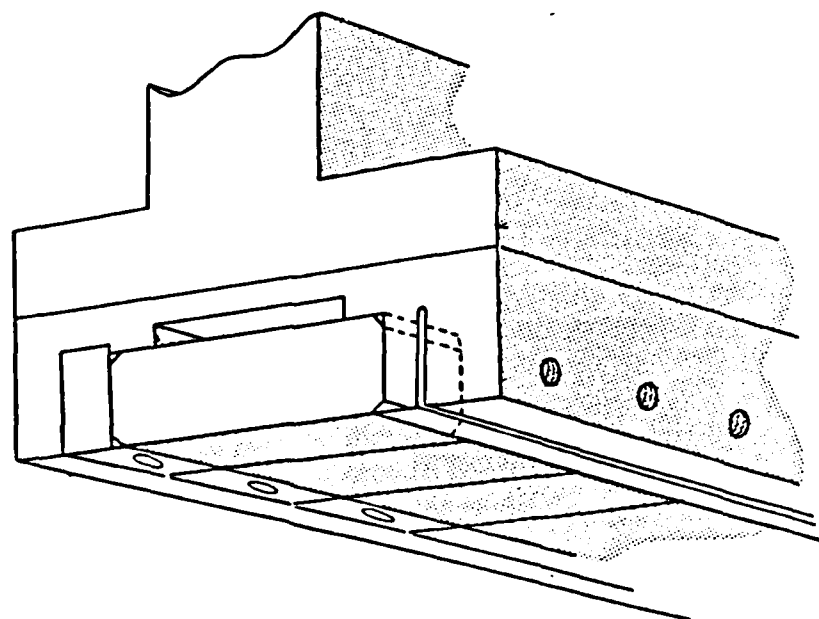
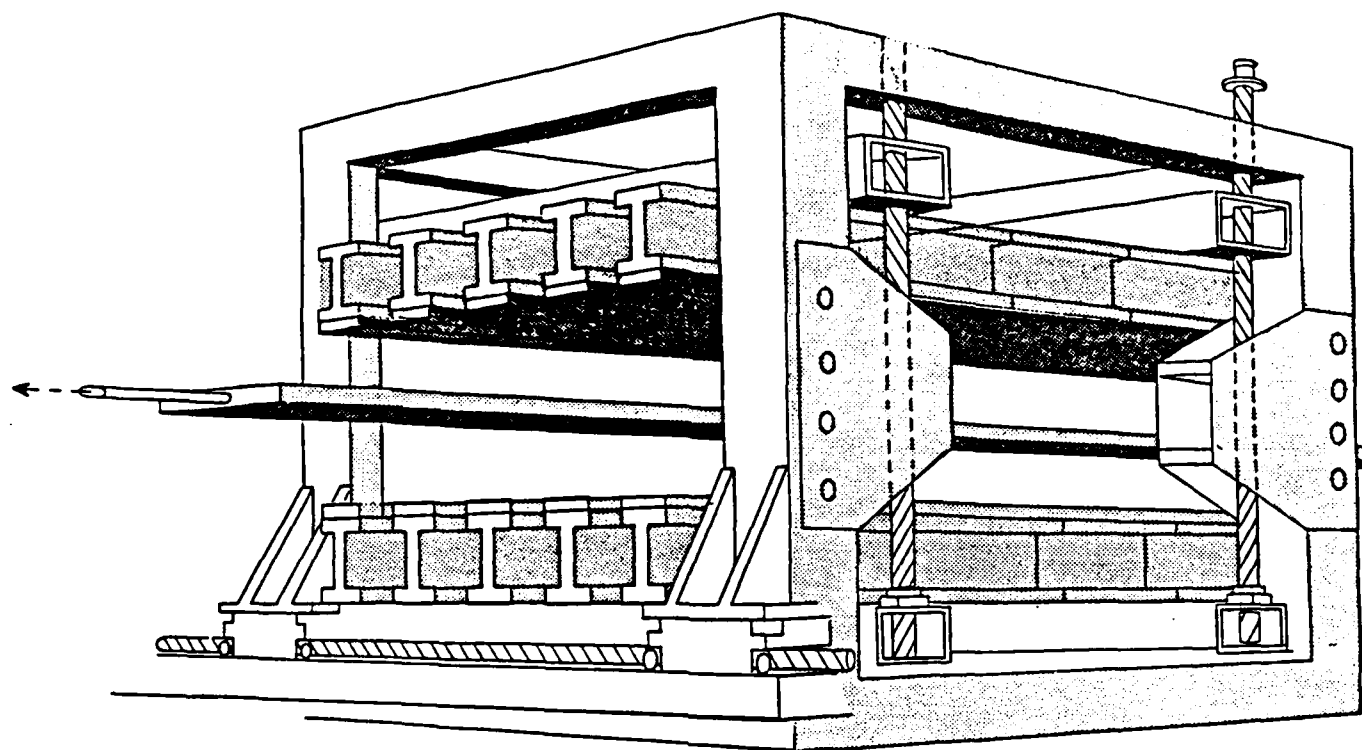


Figure 1

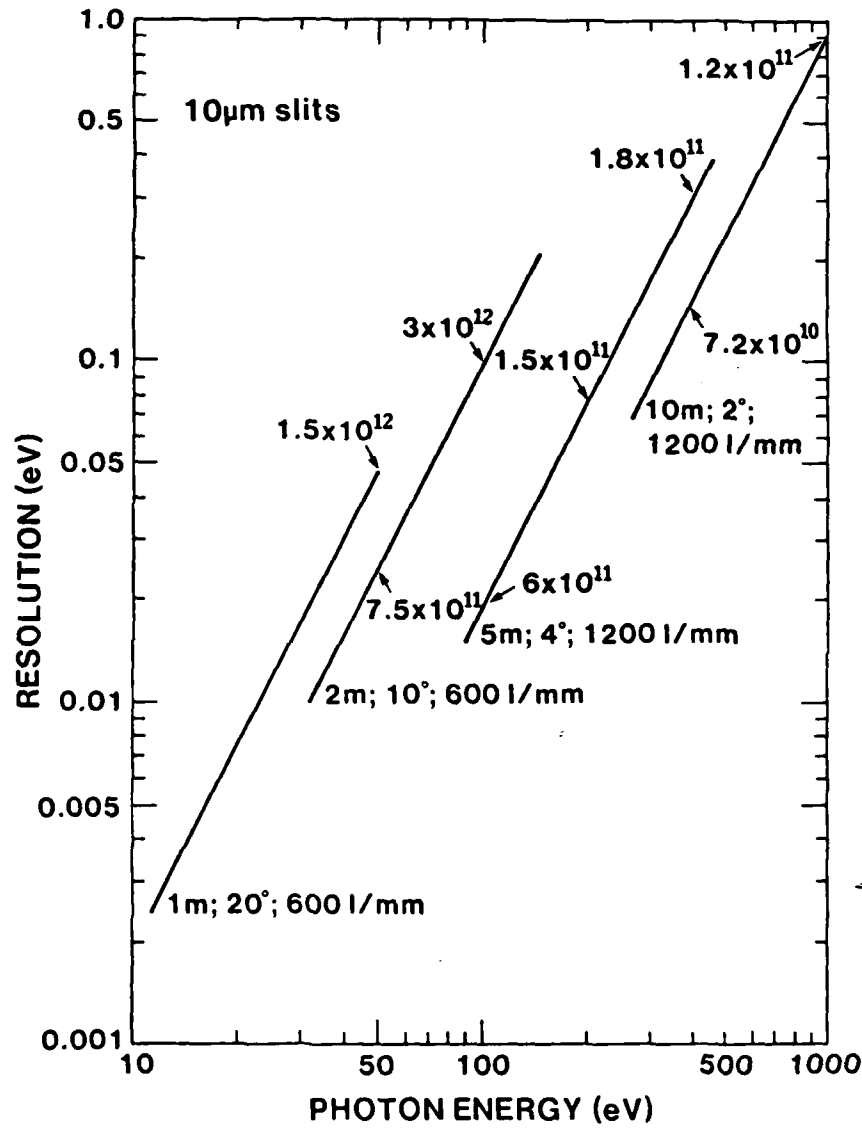


Figure 2

## LOCUST MONOCHROMATOR

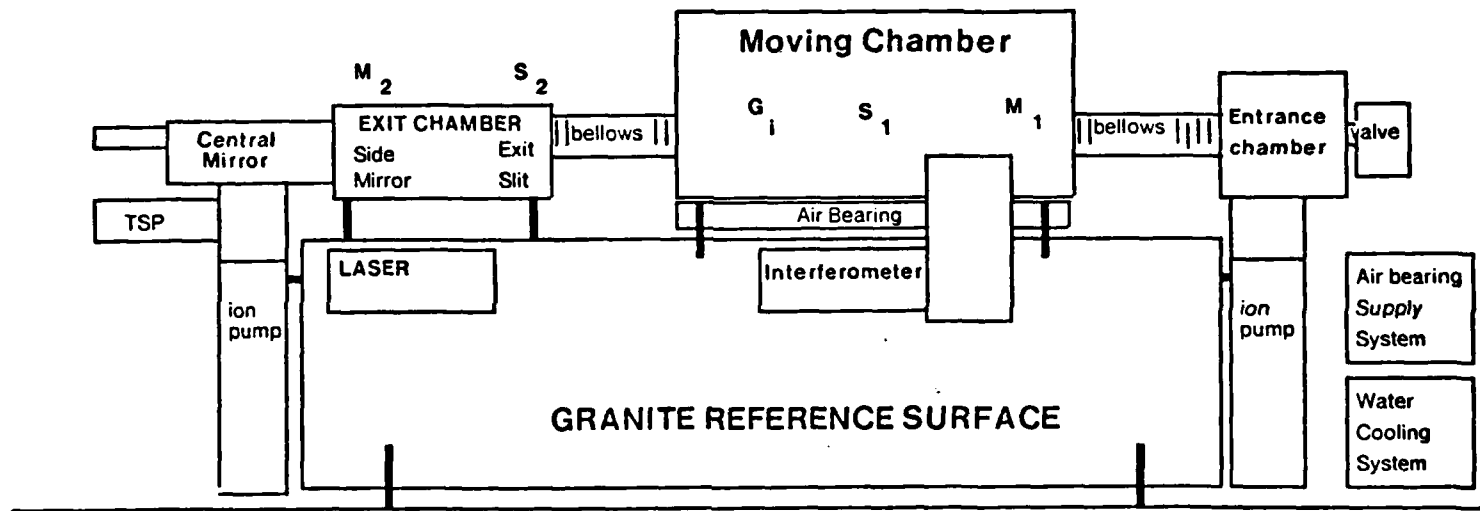


Figure 3

## MOVING VACUUM CHAMBER

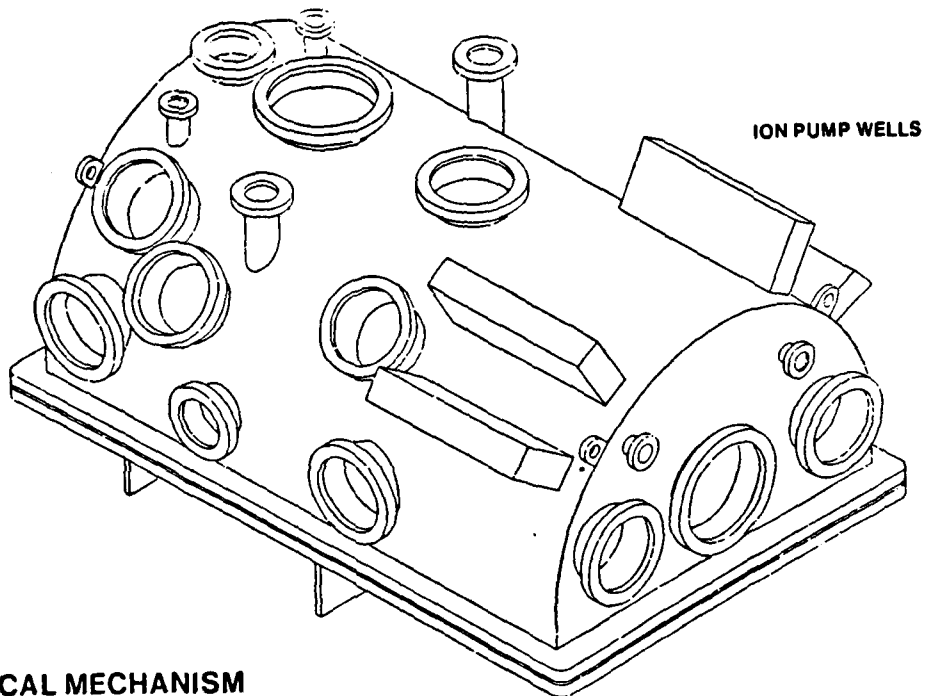


Figure 4a

## OPTICAL MECHANISM

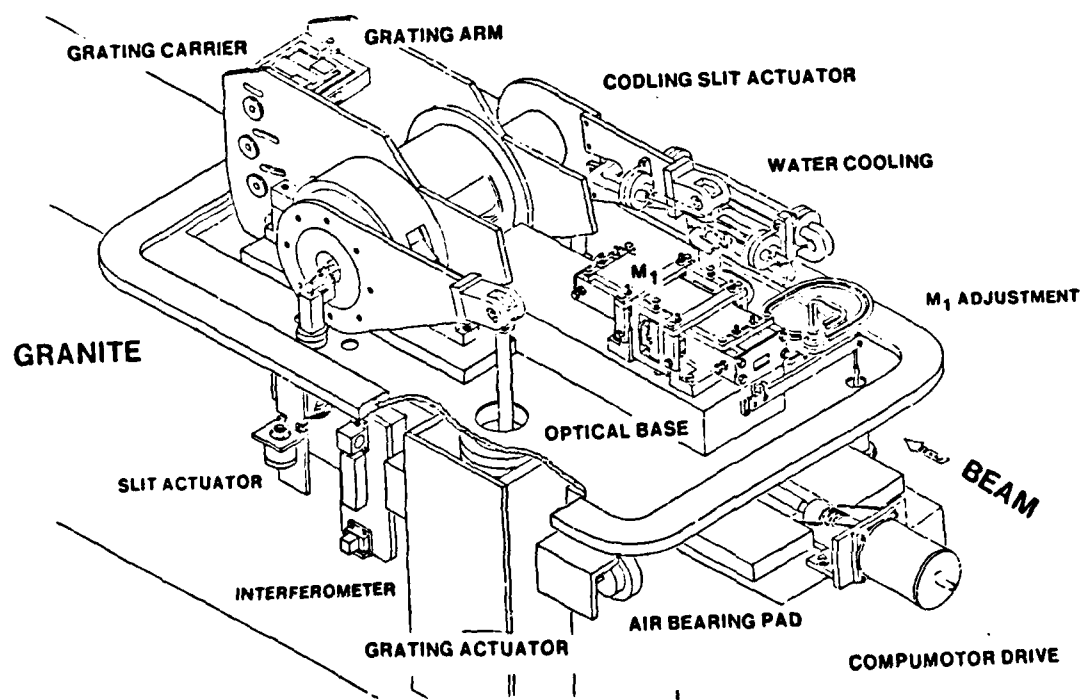


Figure 4b

## BEAM LINE V COMPUTER

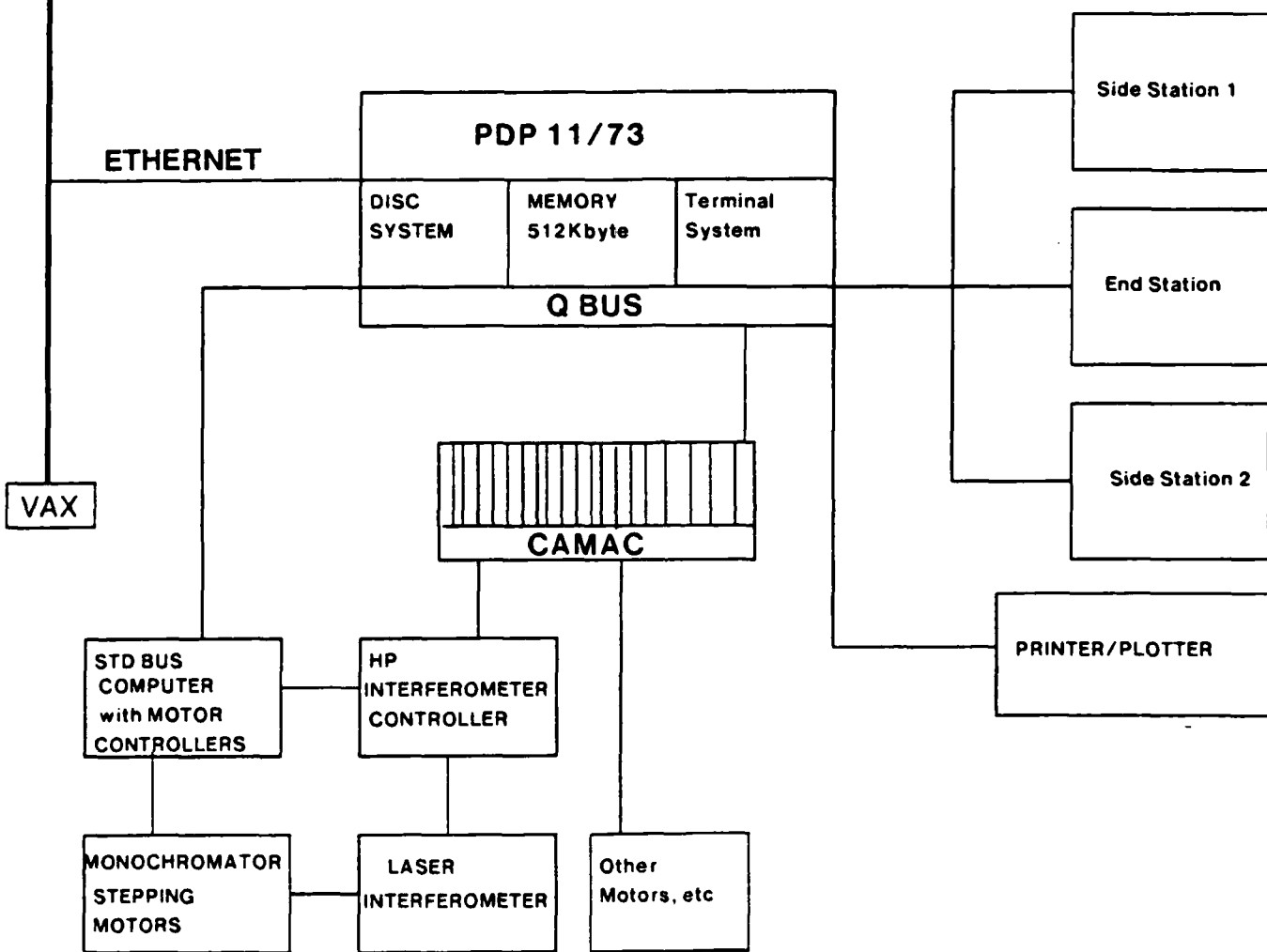


Figure 5

APPENDIX  
INTERNATIONAL CONFERENCE ON INSERTION  
DEVICES FOR SYNCHROTRON SOURCES  
(R. Tatchyn and I. Lindau, eds.)

**The SSRL Insertion Device Beam Line 'Wunder'**

R.Z. Bachrach and R.D. Bringans

Xerox Palo Alto Research Center  
3333 Coyote Hill Road, Palo Alto, Ca 94304, (415)494-4157

B.B. Pate and R.G. Carr

Stanford Synchrotron Radiation Laboratory  
SLAC Bin 69, PO Box 4349, Stanford University, Stanford, Ca 94305

**Abstract**

Insertion devices as radiation sources on storage rings offer potential for substantial gains in beam brightness and flux delivered to a sample. Achieving these gains, however, requires several new aspects of beam line design. New aspects of beam line design arise from the high beam power, the complex spectral and geometrical characteristics, and the need for a wide spectral range. We discuss these aspects of insertion device soft X-ray synchrotron radiation beam lines with examples drawn from our project creating Beam Line Wunder at the Stanford Synchrotron Radiation Laboratory. The major research use envisioned for this beam line is for spectroscopic experiments which require the highest possible intensity and resolution for a tunable constant deviation source. We summarize the current status of each of the beam line major components: the Multi-undulator, the transport system, the Locust Monochromator, the computer control system, and the experimental area.

**I. Introduction**

Several new aspects of synchrotron radiation beam line design become important when bending magnet sources are replaced by an undulator. Our project creating Beam Line Wunder at the Stanford Synchrotron Radiation Laboratory<sup>1,2</sup>, SSRL, has illucidated and evaluated these aspects for their impact on all the beam line system elements. In this paper, we describe the requirements for an undulator based beam line in the context of the formulation of SSRL Beam Line Wunder. We review specific detail on the designs and implementations aimed at a beam line for the spectral range from 10-1000 eV which will deliver the highest possible power density to the sample in the smallest feasible bandwidth.

The primary system concerns can be partitioned into beam collimation, spectral range, spatial characteristics, and power. In particular, the increased beam power density from an undulator source necessitates active cooling of most elements likely to be hit by the beam. In the case of optical elements, this requirement arises not only because of possible damage, but also because distortions of the optics must be minimized to maintain ultimate performance. As a result of our studies, we have shown a new way for configuring undulators as sources, we have shown the expected improvements to be gained from silicon carbide optics, we have formulated a state of the art second generation soft X-ray monochromator which can handle the high power and deliver high resolution, and we have resolved issues on the best experimental configurations for the use of undulator beams.

## The SSRL Insertion Device Beam Line 'Wunder'

R.Z. Bachrach and R.D. Bringans

Xerox Palo Alto Research Center

3333 Coyote Hill Road, Palo Alto, Ca 94304, (415)494-4157

B.B. Pate and R.G. Carr

Stanford Synchrotron Radiation Laboratory

SLAC Bin 69, PO Box 4349, Stanford University, Stanford, Ca 94305

### Abstract

Insertion devices as radiation sources on storage rings offer potential for substantial gains in beam brightness and flux delivered to a sample. Achieving these gains, however, requires several new aspects of beam line design. New aspects of beam line design arise from the high beam power, the complex spectral and geometrical characteristics, and the need for a wide spectral range. We discuss these aspects of insertion device soft X-ray synchrotron radiation beam lines with examples drawn from our project creating Beam Line Wunder at the Stanford Synchrotron Radiation Laboratory. The major research use envisioned for this beam line is for spectroscopic experiments which require the highest possible intensity and resolution for a tunable constant deviation source. We summarize the current status of each of the beam line major components: the Multi-undulator, the transport system, the Locust Monochromator, the computer control system, and the experimental area.

### I. Introduction

Several new aspects of synchrotron radiation beam line design become important when bending magnet sources are replaced by an undulator. Our project creating Beam Line Wunder at the Stanford Synchrotron Radiation Laboratory<sup>1,2</sup>, SSRL, has illucidated and evaluated these aspects for their impact on all the beam line system elements. In this paper, we describe the requirements for an undulator based beam line in the context of the formulation of SSRL Beam Line Wunder. We review specific detail on the designs and implementations aimed at a beam line for the spectral range from 10-1000 eV which will deliver the highest possible power density to the sample in the smallest feasible bandwidth.

The primary system concerns can be partitioned into beam collimation, spectral range, spatial characteristics, and power. In particular, the increased beam power density from an undulator source necessitates active cooling of most elements likely to be hit by the beam. In the case of optical elements, this requirement arises not only because of possible damage, but also because distortions of the optics must be minimized to maintain ultimate performance. As a result of our studies, we have shown a new way for configuring undulators as sources, we have shown the expected improvements to be gained from silicon carbide optics, we have formulated a state of the art second generation soft X-ray monochromator which can handle the high power and deliver high resolution, and we have resolved issues on the best experimental configurations for the use of undulator beams.

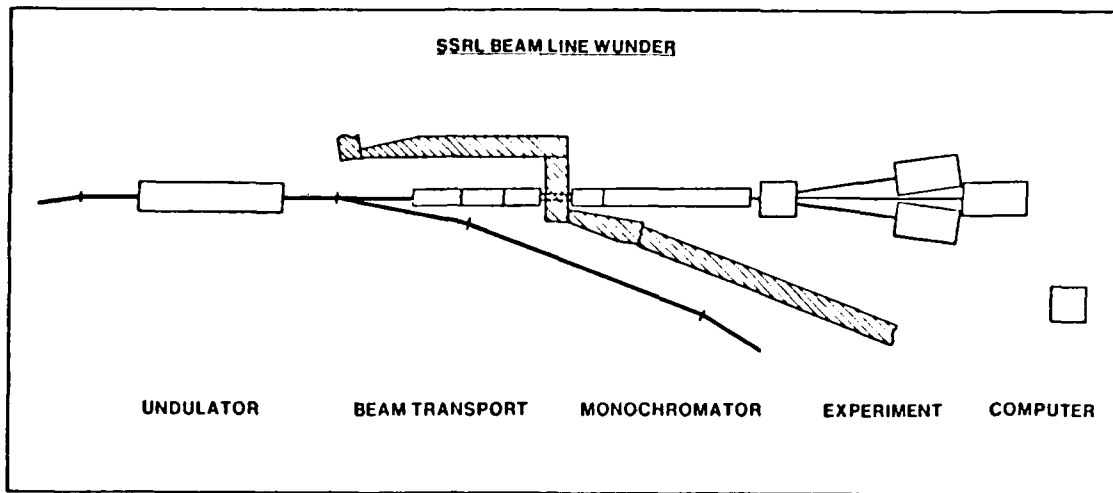


**Fig. 1** Beam line description consisting of the elements: Source, transport, monochromator, experiment, computer.

The project began in 1979 as a bending magnet beam line but shifted to wiggler-undulator technology after the successful operation of a permanent magnet device in SPEAR.<sup>3,4</sup> The collaborative project<sup>1</sup> between Xerox and Stanford motivated the funding from NSF/UIC, DARPA, DOE, and Xerox and then first needed to modify the SPEAR storage ring to free up the physical space for the required straight section by replacing the previous four SPEAR design RF cavities with two of the PEP design. The funding required for the construction and installation of these two RF cavities was substantial and therefore our beam line development work was delayed several years as the initial funding was used to modify the storage ring. In the mean time, we pursued detailed studies both of undulators as sources and of the impact of achieving the desired performance with the high powers anticipated before embarking on specific designs.<sup>2</sup> These studies led us to the beam line system implementation described here.

Figure 1 summarizes the main beam line elements that are discussed in this paper. The Xerox/Stanford SSRL BLV Multi-undulator; the beam transport system; the Locust Monochromator; the experimental area; and the beam line computer. We will discuss aspects of each of these elements in that order, but these descriptions should be considered previews until operational data is available in the next year to two.

## II. The Xerox/Stanford SSRL BLV Multi-undulator

Early in the design studies of the beam line,<sup>1,2</sup> we specified that several undulator periods would be required to span fully the design range of 10-1000 eV. The result of the considerations is the discovery that specific insertions could be sized so that they could be placed close together. Scanning the undulators can be accomplished in a straightforward manner by varying the magnet jaw gaps of all the undulators simultaneously with the active one positioned over the SPEAR beam pipe. Interchange between the different periods can then be carried out by opening the jaws to full gap and sliding the undulators across the beam pipe within the confines of the SPEAR tunnel. The resultant Xerox/Stanford SSRL BLV Multi-undulator, shown in figure 2 with five possible insertion devices, was installed into SPEAR on September 10, 1985, and its construction and operation will be detailed in a subsequent paper. Table 1 lists many of the relevant parameters. Figure 2 depicts the five possible insertion devices mounted on individual stainless steel I beams mounted in the mover structure surrounding the SPEAR beam pipe. The inset shows how the SmCo<sub>5</sub> magnet bars are held

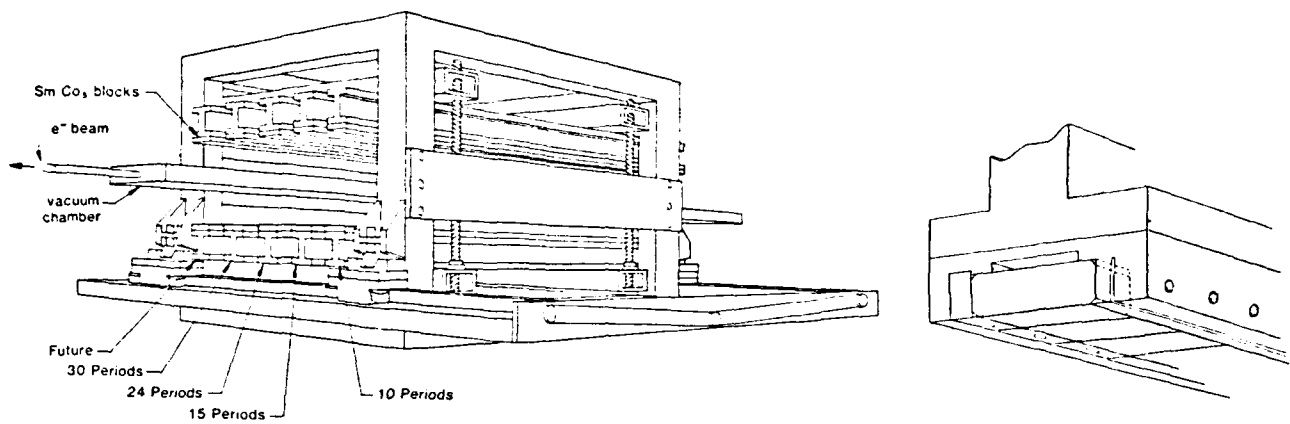


**Fig. 2** Pictorial of the Xerox/Stanford SSRL BLV Multi-undulator. The five possible insertions mounted on stainless steel I beams are shown installed in the mover assembly surrounding the SPEAR beam pipe. The inset shows how the SmCo<sub>5</sub> magnet bars are mounted.

TABLE I  
Xerox/Stanford SSRL BLV Multi-Undulator Parameters

|   | Length: 183 cm                        | Minimum Gap: 3cm                      | SPEAR: 3.0 GeV 100ma                  |
|---|---------------------------------------|---------------------------------------|---------------------------------------|
| Number of periods                           | 10                                    | 15                                    | 24                                    |
| Period Length- $\lambda$ (cm)               | 18.3                                  | 12.2                                  | 7.6                                   |
| Magnet Block Size (cm)                      | $\lambda/8 \times \lambda/8 \times 8$ | $\lambda/8 \times \lambda/8 \times 7$ | $\lambda/4 \times \lambda/4 \times 6$ |
| Tuning Range* (eV)                          | 16-417                                | 84-622                                | 360-1020                              |
| K maximum (3 cm gap)                        | 9.0                                   | 4.6                                   | 2.6                                   |
| E <sub>1</sub> , P <sub>tot</sub> (max K)   | 11.3, 289.4                           | 59.8, 173.2                           | 260.7, 136.3                          |
| E <sub>1</sub> , P <sub>tot</sub> (K = 3.5) | 65.8, 56.6                            | 99.0, 98.5                            | ..                                    |
| E <sub>1</sub> , P <sub>tot</sub> (K = 1.4) | 237.5, 7.3                            | 356.3, 16.4                           | 570.0, 42.0                           |
| E <sub>1</sub> , P <sub>tot</sub> (K = 0.5) | 417.0, 0.9                            | 621.6, 2.0                            | 993.4, 5.0                            |
| E <sub>1</sub> , P <sub>tot</sub> (K = 0.0) | 467                                   | 700.8                                 | 1120.6                                |
| eV, watts                                   | eV, watts                             | eV, watts                             | eV, watts                             |

\* The lower limit of this tuning range is set by the beam line power limit. With suitable power filtering, the maximum K range can be reached. Note that if the storage ring energy is reduced these number scale by the square of the energy.

The Multi-undulator innovation represents a major advance in the art of permanent magnet undulator devices and solves the problem of achieving a wide range while remaining in the undulator regime. We have chosen to implement devices with N=10,15,24 and 30 periods in the available 183cm SPEAR straight section corresponding to 18.3, 12.2, 7.6, and 6.1 cm period lengths.

The undulator devices implemented use the permanent magnet arrangement described by Halbach<sup>5</sup> in which there are M=4 blocks per undulator period. The relationship between the on-axis field, the magnet gap g, magnet height h, magnet period  $\lambda$ , and the remanent field  $B_r$  of the magnets is given by:

$$B_0 = 2 B_r \exp[-\pi g/\lambda] \frac{\sin(\pi/M)}{\pi/M} [1 - \exp(-2\pi h/\lambda)] \quad (4)$$

In the limit where the dimension of the magnets transverse to the beam is large. The magnets we have received from Vacuum Schmelze achieve 0.93 Tesla for  $B_r$ . We have restricted ourselves to an out of vacuum device and thus the minimum gap for the magnets is about 3.0cm. In optimizing our devices, the 30 and 24 period devices have  $h = \lambda/4$  while the 15 and 10 period devices have two square section blocks with  $h = \lambda/8$  per orientation. This reduces the maximum field and thereby K and power. The length of the blocks was also made as small as feasible consistent with the magnetic field uniformity required for operation of the storage ring. One should note that reducing the volume of SmCo<sub>5</sub> for these latter devices represents a substantial reduction in cost. In assembling the magnets, a number of constraints were developed to sort and place the individual magnets. The sorting procedure is described in this volume<sup>6</sup> and the overall construction of the Multi-undulator will be presented in a subsequent paper.<sup>7</sup>

The combination of periods achieves the scanning ranges for  $E_1$  depicted in figure 3 (reproduced from reference 2) for SPEAR operating at 1.5 and 3.0 GeV and derived from equation 1 for the  $i$ th harmonic.

$$E_i(\text{eV}) = \frac{950 [E_s(\text{Gev})]^2}{\lambda(\text{cm}) [1 + K^2/2 + \gamma^2 \theta^2]} \quad i=1,2,3,4, \dots \quad (1)$$

The parameter  $K$  is defined as:

$$K = 0.934 B_0(\text{Tesla}) \lambda(\text{cm}). \quad (2)$$

$B_0$  is the on axis magnetic field,  $E_s$  is the stored electron energy,  $\gamma = E_s(\text{MeV})/0.511$ , and  $\theta$  is the observation angle. One can think of  $K$  as a coupling constant that expresses how much the electron beam is being wiggle. Small  $K$  corresponds to the undulator regime and high  $K$  to the wiggler regime. In optimizing the undulator design for the photon energy range of 10 to 1000eV at an electron energy of 3.0GeV several considerations arise. For example, for the original 30 period device installed at SSRL, the fundamental cannot go below about 720eV in an out of vacuum mode. Increasing the length of the undulator's period makes this problem less severe but reduces the overall intensity in a fixed length device because of the reduction of the number of periods. With the length limitation that  $N\lambda$  must be less than about 183cm one can see from equation (1) that high values of  $K$  and/or  $\theta$  are required in order to get down to lower photon energies. The 15 period device covers much of the desired range, but the coverage and overlap is improved by having the 10 and 24 period devices. The 10 period device in particular makes the low energy range accessible with the first harmonic. For SPEAR at 3 GeV, pushing the fundamental below 50eV even with the 10 period device requires large values of  $K$  and thus high total power from the device.

In an earlier study<sup>8</sup> some of these aspects were examined and plots were given of the magnet jaw gap size and the magnitude of  $K$  required to obtain a particular value of the first harmonic. Figure 4 presents this information with the parameters from the implemented Multi-undulator periods. Shown are the energy of the first harmonic and  $K$  as a function of undulator jaw gap for the four undulators. The gap drive system was designed with sufficient resolution that both the Multi-undulator and the monochromator can track together. This required a stepping tolerance of about 25μm

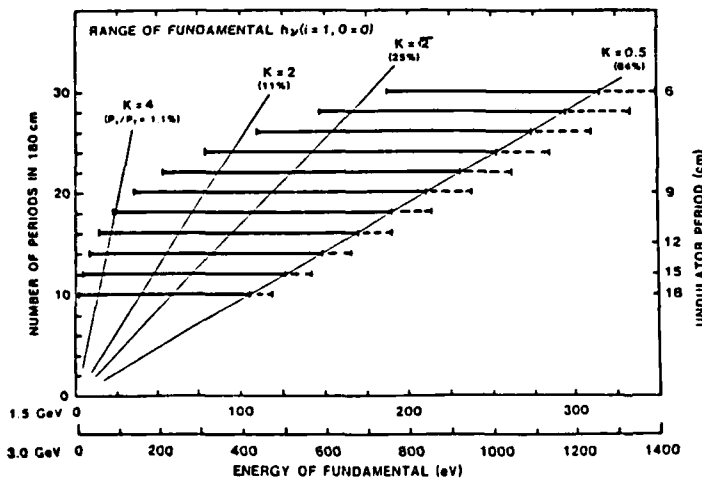


Fig. 3 Diagrammatic representation of tuning ranges for wiggler-undulators showing the consideration of parameter adjustments. The two axes are the number of periods and the energy of the fundamental for SPEAR operating at 1.5 and 3.0 GeV. At present, 10, 15, 24, and 30 period devices have been constructed and provide a set of overlapping ranges spanning 10-1000eV.

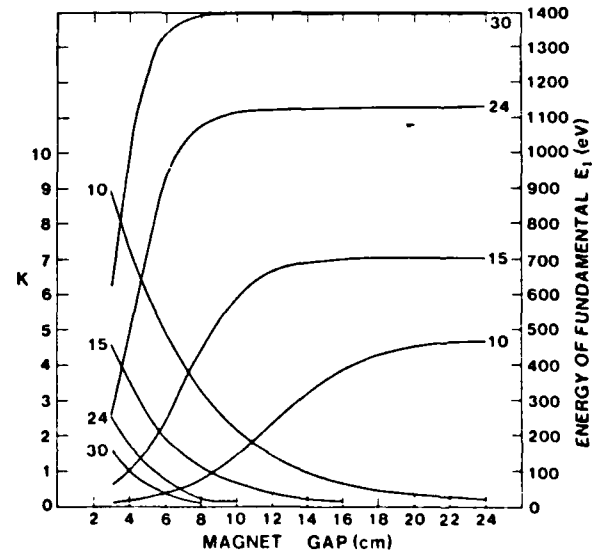


Fig. 4 Plot of  $K$  and energy of the fundamental versus magnet jaw gap for the four multi-undulator periods.

In previous papers, we have characterized our expectations for the power from these devices. Figure 5 compares the expected first harmonic flux for three of the undulators compared to bending magnet and wiggler devices. The undulator curves depict the first harmonic tuning range while the wiggler and bending magnet curves are continua. The total power radiated by the undulator per mA of electron beam current is given by<sup>2</sup>.

$$P_T (\text{W/mA}) = 0.00730 K^2 [E(\text{GeV})]^2 N / \lambda(\text{cm}) \quad (5)$$

and the power in the fundamental is given by the approximate equation

$$P_1 \approx P_T / (1 + K^2/2)^2 \quad (6)$$

This relationship is shown graphically in Figure 6. Note that to a good approximation, the first harmonic power peaks at  $K = \sqrt{2}$  where it equals one quarter the total power. In general, if one can tolerate the total power loading, one can for a fixed length device usually get more power at the photon energy of interest by operating a short period device at a higher  $K$  value. Thus the design optimization criteria are fairly complicated and involve a lot of system considerations which include both spatial and spectral filtering. For the Beam Line Wunder design, the determining criteria ultimately were set by the power handling capability and the aperture of the monochromator. We thus limited the ultimate capability of elements in front of the monochromator to match and thereby limited the cost. The major design objective is to achieve as wide a range as possible while keeping the  $K$  parameter below 2 in order to stay in the undulator regime as much as possible. The undulator regime is desirable because it optimizes the flux at the desired energy to the total flux.

We show in Figure 7 selected spectra calculated for  $K = 1.25, 2.25$ , and  $3.5$  for the 15 period undulator which, with suitable scaling of the energy and intensity scales, are typical of those for any of the devices over the same  $K$  range. The spectra are the result of integrating over all azimuthal angle  $\varphi$  and over  $\theta$  up to a maximum angle of 1 mrad. The assumption that the emittance of the electron beam is zero has only a small effect when integrating over such large angles. The general trend is that as  $K$  increases, the continuum aspect increases but that there is significant modulation of the spectrum. Below  $K = 1$ , the spectrum is essentially dominated by the first harmonic. Note that in all the spectra, the low energy cut off energy is the same and is established by the viewing aperture.

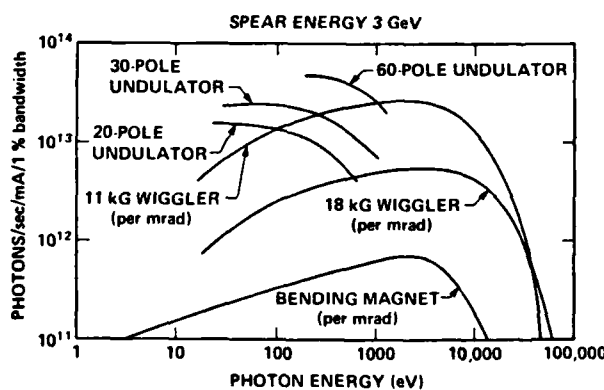


**Fig. 5** Estimated first order flux into the beam line for various sources for SPEAR operating at 3GeV under dedicated conditions. The wiggler and bending magnet curves are a continuum. The undulator curves represent a tuning range with the low energy cut off determined by the minimum gap between the permanent magnets. This range also shifts with the stored energy of SPEAR beam.

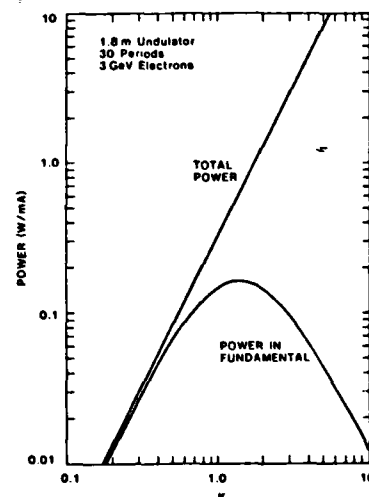
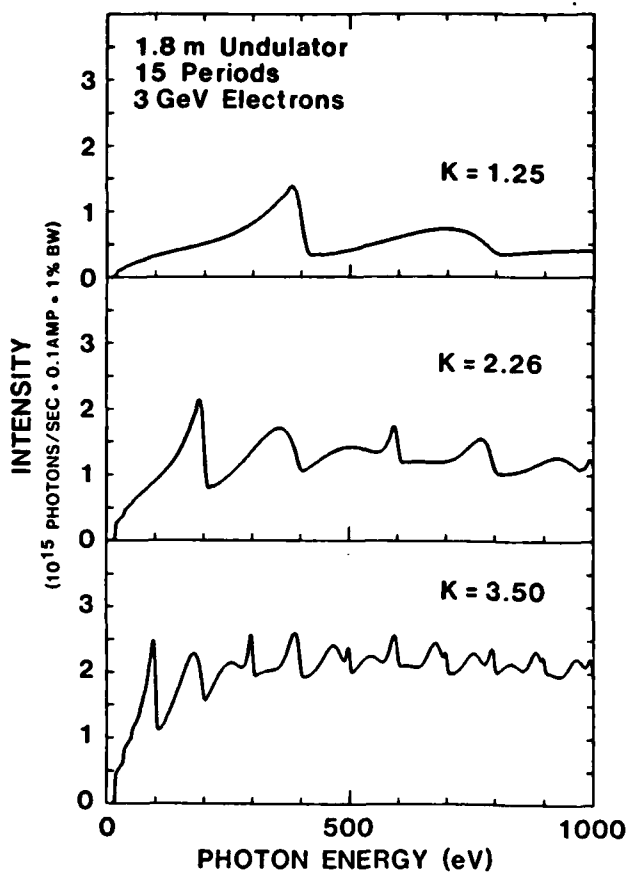


**Fig. 6** Comparison of total power and power in the first harmonic as a function of  $K$  showing the optimization in the vicinity of  $K = 1$ . One should note however that the total optical power at a desired energy can be increased by increasing  $K$  if one can handle the total power.

**Fig 7** Undulator spectra for a 15 period undulator with  $l = 12.2\text{cm}$  period length for SPEAR operating at an electron energy of 3 GeV. Spectra are shown for three values of the undulator parameter  $K$ , ie three different magnet jaw gap settings.



To obtain photon energies below about 60 eV with the 15 period device, it is necessary to go to large observer angles. Because the beam line elements, in particular the gratings in the monochromator, subtend a finite angle, it is important to examine the effect of an angular restriction on the spectra. In the spectrum for  $K = 3.5$  the angular cutoff is seen clearly as the step like structure at low energies. It is clear that the constraints for Beam line V at SSRL require that relatively large acceptance angles be available in order to get to low photon energies with the 15 period device. One can extend the range however by working in the tail of the first harmonic. As can be seen in figure 7, the first harmonic has a considerable tail to low energy. Spatially, these lower energy components arise off axis and so if one wants to use them, one needs to collect a larger solid angle than needed for the first harmonic energy. Ideally one would extend to 3 milliradians in the horizontal, but for a number of reasons we limited this implementation to 1.5 milliradians. We propose to obtain the wider range if necessary with the power filter described below.

Examination of the spectra for the 15 period undulator in figure 7 shows that it is easy to cover the range from ~20 to 1000 eV with one setting (e.g.  $K = 3.5$ ) if one does not require the fundamental to be scanned. It is clear that careful monitoring of the incident photon flux and good higher order rejection would be necessary for spectroscopic experiments in this case because of the intrinsic modulation of the input beam. To scan the fundamental over a similar range requires the full complement of devices.

Table 1 summarizes the parameters characterizing the Multi-undulator for SPEAR operating at 3GeV, a typical dedicated operating condition. For each device the range of the fundamental will have a low energy cutoff set by the requirement that the magnets have a remanent field of 0.93 Tesla and a minimum gap of 3.0cm, and an absolute high energy cutoff set by  $K = 0$  in equation (1). Table one shows the tuning ranges achievable with the Multi-undulator based upon power criteria and also characterizes the photon energy and radiated power at  $K$  values of 3.5, 1.4, and 0.5 corresponding to the half power and maximum of the fundamental.

In the principal operating mode, the SPEAR control room will enable the Beam Line V computer to control the variation of the magnet jaw gap within appropriate limits. The dual control system also allows the Multi-undulator to be operated from the SPEAR control room when appropriate. Some of these aspects are discussed further in section VI.

### III. BEAM TRANSPORT SYSTEM

The beam transport system is the backbone of the beam line and incorporates a number of essential elements for beam forming, control, and diagnostics. A previous paper outlined the functional elements required in detail<sup>2</sup>. Initially we had hoped to utilize a rather small diameter pipe, but more detailed examination of the spatial characteristics of the beam and issues of radiation safety led us to a design that was more typical of bending magnet transport systems. Avoiding transitions in flange sizes is also advantageous, so that we propagated a given pipe size until a transition was necessary for other reasons.

A series of masks, stoppers, valves, shutters, and apertures constitute the initial control part of the beam line. The masks serve to protect the valves from the beam power loading and also act as radiation shields. The stoppers are an absolute radiation shield and are designed to absorb the full beam should it accidentally dump down the beam line. The apertures define the useful beam and in the case of an undulator beam line, also serve to spatially filter stray radiation from upstream bending magnets. This stray source of radiation is a severe problem for position monitor design and for the control of the beam in the vicinity of the beam line takeoff. Our original design specification called for two sets of adjustable apertures, one in front of the position monitor and one after. The later set of apertures can spatially filter the undulator radiation and is useful for isolating the first harmonic and reducing extraneous higher order power. This is a particularly useful aspect with the Multi-undulator. The four periods we have available potentially allow us to drive the first harmonic over the full 10-1000 eV range.

The beam line has both horizontal and vertical steering, but only the vertical steering is maintained with a feed back system. The SPEAR beam position detector consists of a set of 1mm electrodes set 1cm apart in the fringe field of the radiation. This positioning was chosen to accommodate the spatial variation of the undulator beam over the range of operating parameters. The spatial extent of an undulator beam varies enormously, so horizontal position detection, in particular, is difficult. The SPEAR beam is currently 6mmx1mm, so that some horizontal sensing can be accomplished, but this is primarily done with intermittent use of fluorescent screens in the diagnostic sections. The position monitoring and steering is still being evaluated because of overlap of radiation from upstream bending magnets with the undulator radiation. It is hoped that apertures that have been designed but not yet installed in front of the beam position monitor will resolve this problem.

The power limits for the transport system were set by cost considerations. In order to be able to use standard water cooling we set 1200 watts/cm<sup>2</sup> as an upper limit for any element in the beam line with the understanding that the K of the undulators could be restricted to stay below this power limit. For design purposes and until operational experience is gained, we set the maximum power handling capability of the monochromator entrance slit at 40 watts or 40 watts/cm assuming that all the incident power is absorbed in some worst case alignments. This than corresponded to an input power onto the entrance mirror of about 100 watts and was consistent with the grating not absorbing more than 5 watts.

One consideration worth pointing out before proceeding further is that design of a transport for an undulator based beam line would be simpler if one were only dealing with the first harmonic of the undulator which has a relatively simple spatial characteristic. In order to best utilize the full energy and power range of the insertion devices however, one has to allow for operation both on the higher harmonics and, to reach low energies, in the spatially complicated low energy tail of the first harmonic. With all of these aspects considered, the beam line optics needs to accomodate several milliradians of horizontal collection.

In addressing this issue one also has to decide where first to horizontally focus the beam. Because of the characteristics of the undulator source, we chose not to perform any horizontal focusing prior to the monochromator. We then set the aperture of the monochromator at 1.5 mrad to allow collection of the low energy components. Note that if we were just collecting the fundamental, an aperture of 0.5 mrad would have sufficed. The horizontal demagnification on the sample is established by the refocusing optics system after the monochromator. We were also motivated in our choice by the fact that a potential SPEAR upgrade would reduce the beam size by about a factor of two. If we had used a conventional configuration with an M<sub>0</sub> mirror at 8 meters, the power density on the mirror in the undulator mode where the beam divergence is only about 0.5 mrad would have been about 100 times higher than our previous experience. In our current configuration, the first mirror, the elliptical cylinder entrance mirror, M<sub>1</sub>, to the monochromator, is at about 15 meters and is made of silicon carbide.

One way to accomodate the high power present when one increases K is to place a low pass filter before the monochromator. We have considered a variety of schemes, all of which look feasible. The most promising are a vertical deflecting three mirror configuration originally proposed by Rehn<sup>9</sup> and a horizontal Cassegrain configuration proposed by Pate which is both a spatial filter, beam compressor and reflective filter. The latter filter removes the inner 1.5 mrad and compresses the outer 1.5 mrad into the central beam. Both of the schemes allow the beam to enter and exit along the same axis so that little adjustment is needed in the optics for insertion and extraction.

A diagnostics and white light section of the transport system precedes the monochromator. The intent was to accommodate experiments that wanted to use the raw power available without any reflections. It also allows for using the higher harmonics to perform x-ray experiments. This option was discussed in an earlier paper<sup>1</sup> where it was shown that significant flux could be achieved up to 6 or 7 KeV. The diagnostics help to monitor the input flux and beam condition.

#### IV. The LOCUST MONOCROMATOR

In specifying a monochromator for this beam line, we sought an instrument which would match well to the undulator and SPEAR characteristics and which would advance the state of the art. The resulting Locust monochromator implements a constant deviation Vodar geometry Rowland Circle mounting and is descended from the Grasshopper Monochromator.<sup>10</sup> By using closed loop computer control and configurational changes, the design incorporates a number of features that would not be achievable with either the Grasshopper or the Extended Range Grasshopper, ERG,<sup>11</sup> configuration for these optics. One should note that the basic optical path<sup>10</sup> is equivalent in all three of these designs. This descriptive presentation is a preview to a complete presentation which will be made once the instrument is operational. Reference 12 presents a general review of current soft X-ray Monochromators.

##### IVa. Optics Description

One of the principal objectives of the Locust<sup>1,2</sup> was to optimize the working spectral range of 10-1000 eV by incorporating a selectable grazing incidence angle,  $\alpha'$ , on the grating. This approach better optimizes the grating efficiencies over the scanable energy range. It is not possible to optimize such a wide range with a single grating in this mounting. Thus the design incorporates four gratings with different grazing angles of incidence and optimized for subranges as shown in Table 2. This approach has allowed us to satisfy the criteria for blazed gratings that the blaze angle should be small compared to the angle of incidence in order to maintain efficiency.<sup>13</sup> Alternative approaches such as the recent slit-less SX-700 designed by Peterson<sup>14</sup> for BESSY which has a small emittance and the UMO proposal by Brown and Hulbert<sup>15</sup> would not work well on SPEAR.

The optical path for the Locust monochromator shown in Figure 8 consists of a vertically focusing silicon carbide elliptical cylinder entrance mirror,  $M_1$ , a silicon carbide Codling mirror-slit,  $S_1$ , one of four gratings  $G_i$ , an exit Codling mirror-slit  $S_2$ , and a refocusing mirror. The basic scanning operation translates  $M_1-S_1-G_i$  relative to  $S_2$  while  $G_i$  and  $S_1$  rotate in a  $\theta-\theta/2$  relationship. The three motions are actuated independently under computer control, but are actively encoded with a laser interferometer. With respect to the exit slit  $S_2$ , the grating is traveling along a line defined by  $Y_G = X_{G_i} \tan(\alpha')$  where  $Y_G$  is the distance from the line between slits which is collinear with the input beam axis and  $X_{G_i}$  is the distance from the exit slit to the center of the grating. At zero order,  $X_G = S_{1G_i} \cos(\alpha')$  where  $S_{1G_i} = D \sin(\alpha')$  is the entrance slit to grating distance and D is the Rowland Circle Diameter. (Note that D is also the grating radius of curvature.) By making the exit slit of the Codling mirror type, we were able to keep the refocusing optics fixed for all the different grating angles of incidence. Although we examined a number of schemes to eliminate this reflection, they did not seem advantageous or advisable at this time. Note that the total number of reflections is the same as on current Grasshopper or ERG beam lines because we do not have an  $M_0$  collection mirror.

The equation of motions for this optics can be derived from the diffraction equation and the properties of the Rowland Circle. These are:

$$\lambda = d \cos(\alpha') \{ 1 - X_{G_i} / D \cot(\alpha') - [1 - (X_{G_i} / D)]^{1/2} \} \quad (7)$$

$$X_{G_i} = D \{ \sin(\alpha') [\cos(\alpha') \cdot \lambda / d] + \cos(\alpha') [1 - (\cos(\alpha') \cdot \lambda / d)]^{1/2} \} \quad (8)$$

Where  $X_{G_i}$  is the  $S_1-S_2$  distance and d is the ruling period of the grating or  $1/d$  is the density in grooves/mm.

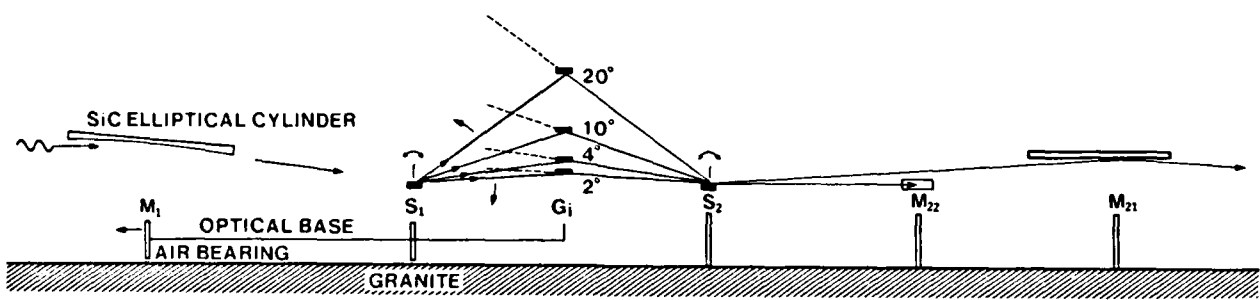


**Fig. 8** Schematic of the Locust optics showing the placement of the elements for a zero order setting. The elements  $M_1$ - $S_1$ - $G_i$  translate on the air bearing relative to  $S_2$ . The motions are coordinated so that as  $G_i$  rotates and translates, the grating travels along the lines emanating from  $S_2$  and the Rowland circle to which the gratings are tangent pass through the two slits  $S_1$  and  $S_2$ .

The basic design approach in the Locust was to make use of the relation for  $S_{IG}$  so that the gratings could be mounted on a common circle and their interchange accomplished by a rotation that is an extension of the primary scanning motion. Our nominal optical design parameters were the set  $(\alpha^*, D)$  equal to  $(2^{\circ}, 10m)$ ,  $(4^{\circ}, 5m)$ ,  $(10^{\circ}, 2m)$ , and  $(20^{\circ}, 1m)$  which established  $S_{IG} \approx 350cm$  and allows all gratings to reach zero order. As discussed below, in the practical implementation, we modified these somewhat and the actual parameters are presented in Table 2. One advantage of this approach is that it allows one to more easily adjust for manufacturing tolerances in the grating radius of curvature which some suppliers quote as loose as  $\pm 5\%$ .

$S_{IG}$  establishes the intrinsic scale of the instrument which is a 10 meter diameter Rowland circle as compared to 2 meters in the Grasshopper and 5 meters in the ERG. This increase in scale enabled us to achieve the desired range using a mechanism encompassed by a vacuum tank with the beam traversing out through a large bellows. One should note that in the ERG or Grasshopper design, the grating mechanism projects into the translation bellows which limits its angular excursion. This feature was a major constraint on the evolution of that configuration. Although the ERG incorporates more than one grating, only one of them can reach zero order. SSRL Grasshopper II has two gratings, but interchange requires subsequent realignment.

A second category of objectives for this implementation was to have all the major aspects of the monochromator under computer control to facilitate experimental use. This includes scanning, slit adjustment, and grating interchange. Grating interchange in other soft X-ray instruments requires manual re-alignment and our approach should avoid that. This feature should facilitate spectroscopic use of the instrument and avoid misconfigurations.

A third category of objectives was to enhance the alignment capability through incorporating appropriate fixtures into the design. Alignment consists of establishing the required spatial relationships of the optical elements to the typically *micron* tolerances required. This includes making the slit to slit axis colinear with the beam axis, centering the entrance slit on the axis of rotation, establishing the slit to grating distance, and placing the grating on the Rowland circle, etc. The tools and facilities built into the Locust design should greatly facilitate the alignment process and go far beyond the capability of the Grasshopper and ERG. The alignment is also facilitated by the incorporation of a three axis interferometer so that the absolute position and rotations are actively directly determined. Alignment systems add complexity to the design, but are appropriate to a second generation instrument such as this.

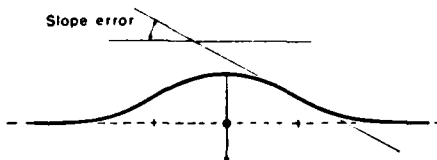
A fourth category of objectives was to incorporate water cooling of the optical elements necessitated by the high input power delivered by the undulator source. The water cooling also needed to have a minimum of loading and vibration effect on the optics and needed to meet construction criteria established by SLAC, namely that there be no water to vacuum welds and that pipes have minimal deflections. One secondary benefit of the water cooling is that it will help thermally stabilize the instrument which is necessary for the ultimate performance.

We presented in a previous paper the results of modeling studies which showed the effect of power loading on the optical elements and presented strategies for minimizing the optical distortion.<sup>2</sup> These are reproduced here as examples of the thermal loading studies. A difficult issue is what design rule to use to estimate the absorbed power for normal and exceptional cases. Particularly in the case of the grating, the problem is likely to be dominated by defects and irregularities. Thermal effects have several aspects which relate to energy, power, and power densities and the capacity of the paths to the sink where it is dumped. In most of our cases, we do not have so much energy that the sink is overwhelmed. We describe the results for two elements: the Codling mirror and the grating.

The Codling slit which is currently implemented in Grasshopper monochromators with SiC because of its better surface roughness capability.<sup>16,17</sup> We needed to estimate the power handling capability of this element for two situations: singly focused vertically to fill the slit and doubly focused horizontally to meet other optical objectives. Thermal calculations are quite difficult for general geometries so Nelson Hower performed model calculations based on some ideal geometries. The present objective is to be able to handle one hundred watts into the monochromator which would give an absorbed power of about 40 watts into the Codling slit in worst case situations. We found that double focused optics which produces power densities of  $10^6\text{-}10^7 \text{ watts/cm}^2$  would damage the entrance slit. We have therefore restricted our considerations to singly focused situations for this monochromator.

Figure 9 presents a schematic representation of the response of the Codling mirror to the focused input power. The table shows parameters for three materials and the distortion response for a back cooled geometry in terms of a slope error. The input parameters were 40 W absorbed or  $7000 \text{ W/cm}^2$  considering the demagnification. With conservative estimates for the mirror reflectivity, this result should correspond to a total power capacity of 100W for our geometry. Whereas quartz would fail catastrophically, SiC seems to be satisfactory to these power densities.

Figure 10 shows the results derived by Hower and Tatchyn for two different strategies for extracting heat deposited in the grating. The results are shown for quartz and then the optimal quartz design is shown with a SiC implementation. For the purposes of this discussion, the variable  $f_p$  represents either the resolving power or the throughput of the monochromator. We do not present the purely radiatively cooled case because the grating temperature would rise to above  $500^\circ\text{C}$  which we considered unacceptable. The back cooled case is very sensitive to the input power because the radius of curvature changes. In fact the optimal solution is to extract the power from the side near the input surface. By keeping the aspect ratio approximately 3:1, this approach uses the cool back to stiffen the structure. The significant improvements are readily seen in the curves. The substitution of SiC for quartz produces the expectation of dramatic improvements in power handling capability. This is principally because of the much better thermal conductivity to thermal expansion ratio ( $K/\alpha$ ) of SiC. Copper or molybdenum do almost as well, but for all of these, the technology of forming gratings has not been established. We are proceeding with quartz gratings in the current implementation, but SiC gratings have recently been reported by Astron.<sup>18</sup>



| $\lambda \text{ (W/cm}^2)$ | $\alpha \text{ (K}^\circ\text{C}^{-1})$ | $F_{\text{opt}}$   | $n_r$ | $T_{\text{max}}$     | $\sigma_{\text{rms}}$ | Slope       |
|----------------------------|---|--------------------|-------|----------------------|-----------------------|-------------|
| SiC 2.0                    | $3 \times 10^{-6}$                      | $6.5 \times 10^8$  | 0.25  | $41^\circ\text{C}$   | 10.6 ppm              | 2.7 arc sec |
| Cu 3.0                     | $16 \times 10^{-6}$                     | $17 \times 10^8$   | 0.34  | $21.5^\circ\text{C}$ | 8.85                  | 8.0         |
| Quartz 0.014               | $0.55 \times 10^{-6}$                   | $10.4 \times 10^8$ | 0.18  | -5400                | 40                    | 37          |

Fig 9. Schematic representation of the response of the codling mirror to the focused input power. The table shows parameters for three materials and the distortion response for a back cooled geometry in terms of a slope error. The input parameters were  $40 \text{ W/cm}^2$  or  $7000 \text{ W/cm}^2$ . Whereas quartz would fail catastrophically, SiC seems to be satisfactory to these power densities. (reproduced from ref 2)

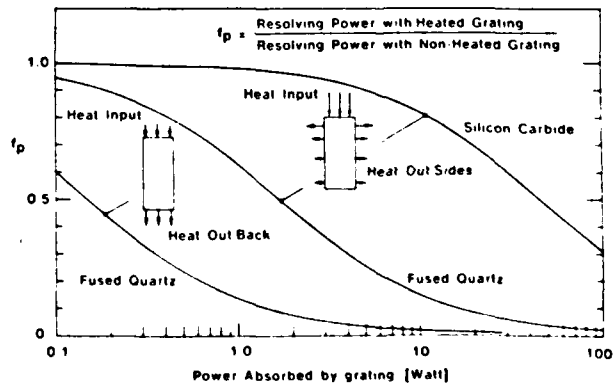


Fig 10. Estimation of throughput degradation from a combined sensitivity analysis of the Rowland Circle optics and thermal calculations. The dominant effect is the change in radius of curvature of the grating with power loading. Three cases are selected for a geometry that is considered near optimal. The two quartz cases compare back and side cooling for quartz. Quartz and SiC are compared for the side cooled case. (reproduced from ref 2)

#### **IVb Configurational Description**

Figure 11 shows the primary configurational elements in the monochromator: the entrance separation chamber; the entrance bellows; the moving chamber; the exit chamber; the air bearing system; the laser interferometer; and the granite reference surface. Figure 12a shows the vacuum chamber while Fig 12b shows the optical mechanism, and the lower half of the vacuum chamber mounted on the granite base. The moving component of the instrument weighs approximately 1300 Kg, but the drive shaft and stepping motor seen in the lower right of figure 12b is capable of driving the mechanism through a single resolution step in less than 50 msec and attain a maximum velocity of about 10 mm/sec. Thus the system can scan its full range in about 1.5 minutes.

The synchrotron radiation enters from the lower right and impinges on mirror,  $M_1$ , a silicon carbide elliptical cylinder being fabricated by TRW<sup>19</sup>. The use of an asphere was motivated by the poor focusing characteristics of the spherical  $M_1$  mirrors used on the original Grasshopper Monochromators. Comparison of spherical, cylindrical, parabolic cylinders and elliptical cylinders using the ray trace program SHADOW developed by Lai and Cerina<sup>20</sup> found that the elliptical cylinder performed best ( $\sigma \leq 20 \mu\text{m}$ ) with our approximately 2 meter undulator extended source. (A similar conclusion for the ERG was found by Hulbert and Brown<sup>11</sup>.) The water cooling pipes are visible on the right. The water pipes were kept as large as possible to minimize vibration that might be induced by turbulent flow. This aspect of mechanical engineering is not well developed, so many of the decisions were based on intuition or other constraints. For example, the gratings are heat sunk well to copper pads which are then connected to the cooling system through flexible braid. The vacuum base and the inner optical base ride on independent air bearings. On the left side are visible the grating angular actuator, part of the laser interferometer optics and the laser beam ports, and then the slit actuator. The Codling slit actuator is on the right side along with the water piping to the slit and gratings. The Codling slit assembly sits within the shaft and the Codling mirror can be removed through the aperture. The grating carriages are mounted between the two arms and have levered adjustment. The grating is mounted in a carrier that is prepared externally. Provision is made for inserting alignment aids during setup. All the connections to the optics come through the base so that the top can be completely removed.

Figure 12a shows the upper part of the vacuum envelope which mates to the flat bottom with a Helicoflex seal. The vacuum chamber is supported independently from the optical mechanism so that any flexing as the system is put under vacuum will not disturb the optics. The ion pumps and Ti sublimation are integrally built into the chamber. The primary ports on the two ends are for the 6"ID entrance and exit bellows. An array of ports allow for monitoring the internal parts, replacement of gratings and alignment without removing the top.

#### **IVc The control system and static and dynamic alignment**

A key aspect of the design is the the control system and incorporation of alignment fixtures. The alignment needs have been principally specified based upon our experience with the SSRL Grasshopper monochromators. The performance objectives of these subsystems was determined by analysis of the sensitivities of the expected performance to tolerance variation and control of the various mechanical parameters. We have gone further in this aspect than previous high vacuum designs in the hope of significantly improving the operational functionality of the instrument. One by-product of our design and the inclusion of alignment and metrology is that this will be the first soft X-ray optical system capable of creating absolute wavelength standards above 100 eV and below the range accessible to crystal instruments.

There are two alignment regimes, static and dynamic. The static regime is established in the initial positioning and phasing of the elements. The dynamic regime consists of maintaining the optical elements in the required spatial positions as they are moved for a scanning operation. The control system needs to move the three axes in a coordinated way such that the elements remain in dynamic alignment.

## LOCUST MONOCHROMATOR

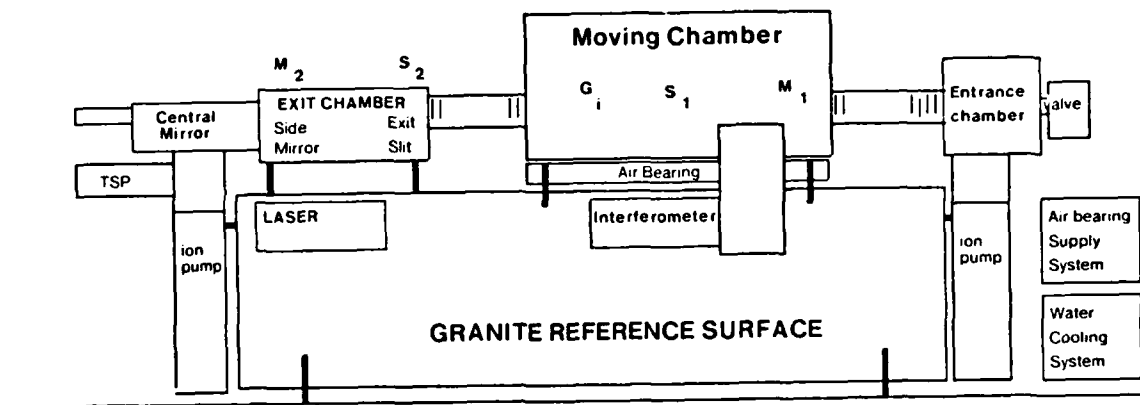


Fig. 11 Schematic side view of the Locust Monochromator showing the major assemblies. The details are given in the text. A perspective view of the Moving Chamber is shown in figure 12. The exit chamber contains the exit slit and the refocusing mirrors.

TABLE 2

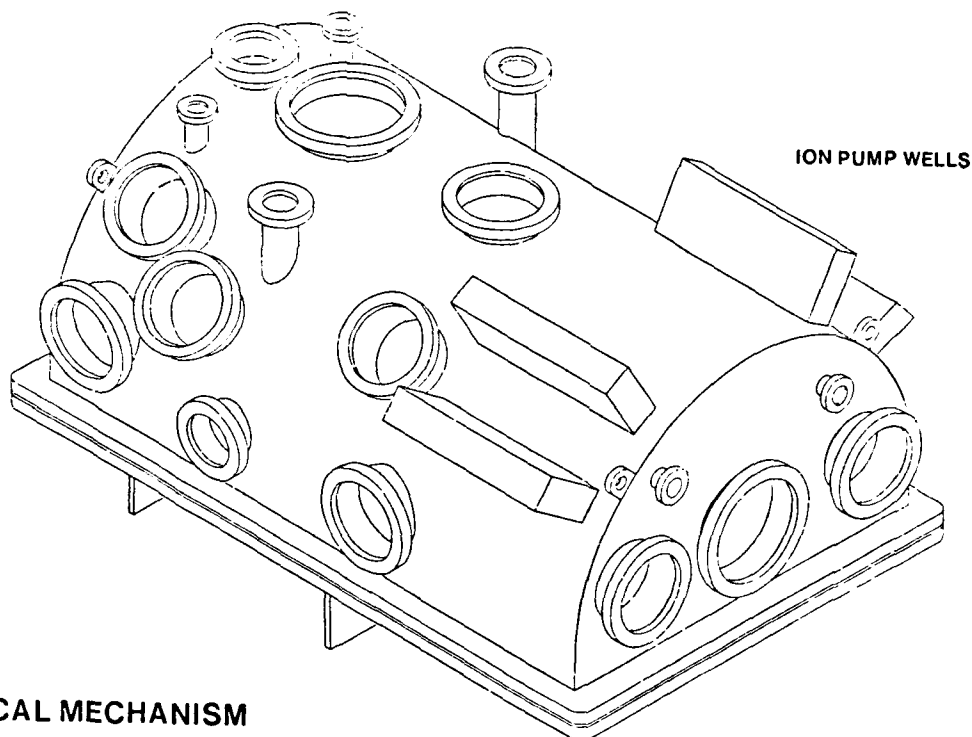
### Locust Monochromator Parameters

Operating Range: 10-1000 eV  
 100 Watts Input Power  
 Silicon Carbide Optics  
 Water Cooled Optics  
 Laser Interferometer Encoding  
 Fully Computer Controlled

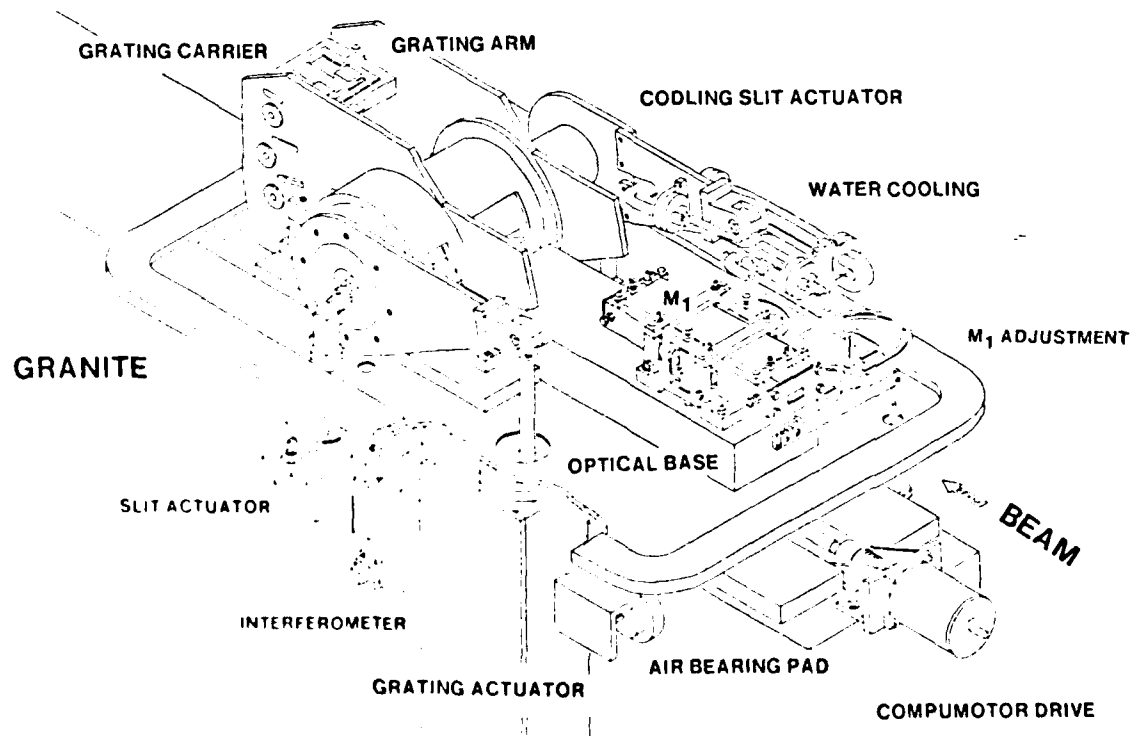
| Grating Angle            | $2^\circ$        | $4^\circ$       | $10^\circ$      | $20^\circ$      |
|--------------------------|------------------|-----------------|-----------------|-----------------|
| Grating Radius (mm)      | 9355             | 4817            | 1986            | 1037            |
| Grating Blank (l.w.d-mm) | 100.40.30        | 80.40.30        | 60.40.30        | 60.40.30        |
| grooves/mm               | 1200             | 1200            | 600             | 600             |
| Resolution (Å)           | 0.0126           | 0.0242          | 0.0593          | 0.1136          |
| $S_{1G}$ (mm)            | 3265             | 3360            | 3448            | 3547            |
| Linear Travel (mm)       | 820              | 800             | 400             | 150             |
| Angular Travel           | $5^\circ$        | $12^\circ$      | $18^\circ$      | $13^\circ$      |
| Blaze angle              | $1.3^\circ$      | $2.0^\circ$     | - -*            | - -*            |
| Blaze Energy (eV)        | 600              | 210             | 70*             | 20*             |
| Resolution at Blaze (eV) | 0.37             | 0.086           | 0.023           | 0.0036          |
| Optimized Range (eV)     | 1500 - 250       | 450 - 90        | 150 - 30        | 50 - 10         |
| Mechanical Range (eV)    | zero order - 220 | zero order - 60 | zero order - 27 | zero order - 10 |

- \* These are laminar cylindrical gratings which are not blazed

## MOVING VACUUM CHAMBER



## OPTICAL MECHANISM



Sensitivity and tolerance studies have been employed to understand critical operational requirements such as grating angle tracking, Codling slit rotation axis centering, granite reference slab flatness, etc.<sup>21,22</sup> Our design is consistent with the requirement that the effect of any one of these isolated errors will contribute an uncertainty of no greater than an energy resolution element ( $10\mu\text{m}$  slits) to the energy calibration of the instrument over its entire scanning range.

In the alignment process, the principal optical axis of the monochromator is determined by the synchrotron beam, the granite reference surface and the  $S_1$ - $S_2$  axis must be made to coincide with this so as  $S_1$  scans over the  $\approx 800\text{mm}$  travel, the deviation from the spatial axis is a minimum. The  $M_1$  mirror needs to be adjusted for optimal focus onto the entrance slit and the slit coordinated with the grating. The grating is statically aligned to place it on the Rowland circle. Once alignment is established, tracking is followed with a Hewlett-Packard three axis interferometer. This primary system is backed up by a set of optical encoders.

#### IVd Ranges and expected performance

Achieving the desired ranges shown in Table 2 was a process of considerable trade off. As the design evolved and configurational implications became clear, we were continually revising the needed and achievable parameters. A major constraint was established by the decision to use a 6" ID bellows for the beam extraction. This limited both the achievable angular range and set the maximal translation limit of 870mm. We thus came up with the ranges presented in Table 2. We describe these ranges as optimized range predicated by the choice of grating blaze which is included between the accessible range. This categorization is useful because all the gratings can go to zero order. Figure 12 shows the resolution versus photon energy over the ranges for each of the gratings. These are accompanied with some flux numbers based upon a theoretical estimate of the monochromator throughput with 100ma in the ring. Note the high resolution over the wide operating range if realized will be significantly greater than that available with most currently operating instruments and competitive with the best ever achieved. The beam spot size on the sample with the optics described below should be about 0.6mm half width at focus.

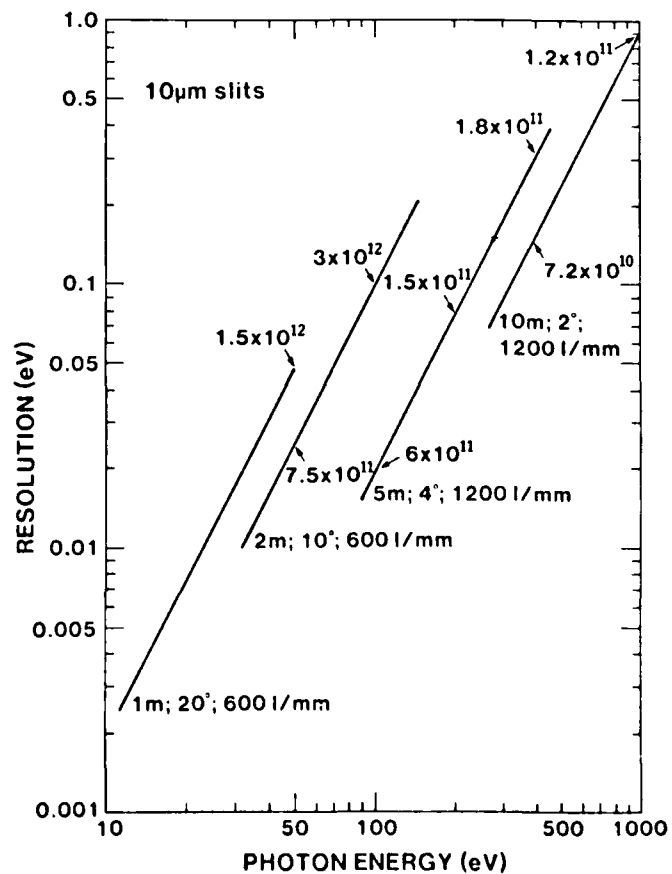


Fig. 13 Estimated energy resolution versus photon energy for each of the gratings. The inset numbers give estimated fluxes at the sample for SPEAR running 100 ma at 3 GeV.

## V. EXPERIMENTAL AREA and REFOCUSING

The Beam Line comprises two basic experimental areas. The first is an approximately one meter long white beam station between the diagnostic section and the monochromator. Although we would have preferred to bring the white beam through the monochromator, no tractable means except setting the monochromator at zero order could be found. The remaining experimental areas come after the monochromator and are created by a filtering and refocusing system built into the monochromator. The exit Coding mirror deflects the beam vertically and then the refocusing system creates the end station and the two horizontally deflected side stations. Before entering the refocusing system, the beam can be filtered either with one or two transmission filters mounted on concentric wheels or with a transmission grating. Since the transmission grating further deflects the beam, this is compensated by adjusting the exit Coding mirror.

The refocusing system thereby creates three work areas by providing two beams deflected horizontally at 14 degrees from mirrors 0.5 meters from the exit slit and one vertically at four degrees with a mirror 1.0 meter from the exit slit. The side stations are at 2.25 meters and the end station 3.5 meters from their respective mirrors. Determining the parameters for these stations was a complicated trade off of a number of parameters since the only optimal solution would have entailed having only one work area. We did consider a number of schemes where chambers were moved around a single port, but they were deemed difficult to implement. Although we would have liked to have moved experimental stations further back, the focusing aberrations substantially increased the size of the beam so that the apertures of typical electron spectrometers would have been overfilled.

The current design plan is based on toroidal optics with evolution to conically formed optics planned in the future. The two side stations have a more limited energy range than the end station, but this is offset by the participating research groups being able to maintain experimental chambers in place permanently. The end station port is for general use and has no permanently installed chamber. Provision has been developed, however, for rapidly changing and positioning chambers including the SSRL facility chambers available for general users.

## VI. COMPUTER CONTROL SYSTEM

The computer system is an integral part of the beam line formulation. Because of the use of closed loop control for coordinating the monochromator, the computer control system is an integral part of the design. All the basic functions of the monochromator are controllable by the computer. In one of the primary scanning modes, the monochromator and the Multi-undulator are scanned simultaneously by the computer.

### BEAM LINE V COMPUTER

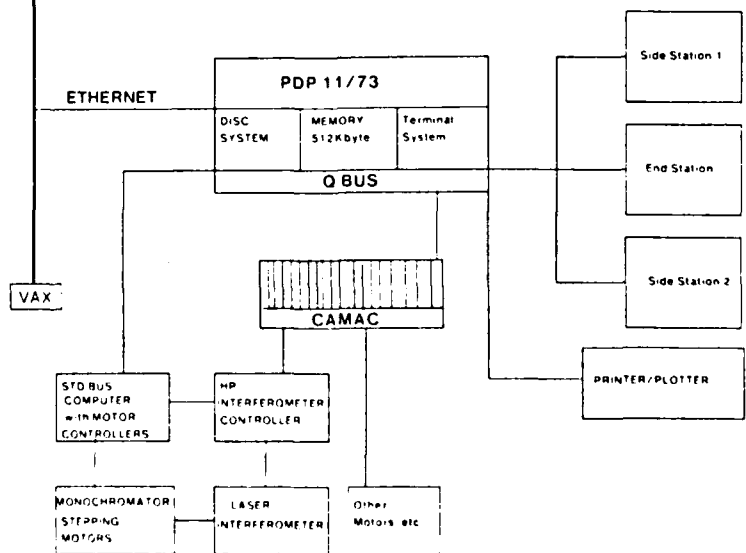


Fig. 14 Schematic of the computer system that will control the monochromator and multi-undulator and will support the three experimental stations. Each experimental station has a terminal and CAMAC crate.

The primary computer is an evolution of our previous PDP11 CAMAC systems using the RSX11M operating system<sup>23</sup> and the XC CAMAC device driver.<sup>24</sup> In the specific implementation, we have used a PDP 11/73 with 512Kbytes of memory, 2 RL02 disks, and an RD52 30 Mbyte winchester. An ethernet system utilizing DECNET connects the beam line computer to the SPEAR control room for operation of the Multi-undulator. We have created three operating stations consisting of terminals and CAMAC crates, one for each of the experimental areas. In order to achieve the control response time desired, a secondary slave microprocessor was implemented for the control of the monochromator stepping motors operated in a feedback loop with a laser interferometer. It interacts directly with the interferometer encoder and the motors during a move operation. The other beam line motor actuators are driven directly from CAMAC.

The CAMAC system also provides a general data acquisition system. A specialized monochromator/undulator task using the XC driver is being developed which will work in coordination with any of the data acquisition and control program in use at SSRL, eg PRG, EXP, and SPECTRA.

**ACKOWLEDGEMENT:** We are indebted to Ingolf Lindau, Art Bienenstock, Bill Spicer and Stig Hagstrom for their efforts on behalf of establishing and their continuing support of the Beam Line V project. A number of people provided key support which enabled us to establish this project in 1981: George Pake and Chuck Hebel of Xerox, Fred Betz, Adrian DeGraaf, and Bill Oosterhuis of the NSF, and Richard DeLauer and Richard Reynolds of DARPA. Nelson Hower and Lars Erik Swartz have made important contributions to the designs. We thank Herman Winick for his interest and for discussion of the Multi-undulator. We thank Brad Youngman for his management of the SSRL BLV Engineering effort and his important contribution to the construction of the Multi-undulator. Jim Montgomery, Richard Boyce, Carl Cork, John Yang, and Harry Morales of SSRL have also made important contributions to the beam line.

This work was supported by NSF/UIC Grant DMR 81-08343 , DARPA, the DOE, and Xerox and was performed at the Stanford Synchrotron Radiation Laboratory and SLAC which are supported by the DOE.

## REFERENCES:

1. R.Z. Bachrach, L.E. Swartz, S.B. Hagstrom, I. Lindau, M.H. Hecht, and W.E. Spicer, Nucl. Inst. and Meth., 208, 105, (1983).
2. R.Z. Bachrach, R.D. Bringans, N. Hower, I. Lindau, B.B. Pate, P. Pianetta, L.E. Swartz, R. Tatchyn, Nuclear Instruments and Methods, 222, 70-79 (1984); also R.Z. Bachrach, R.D. Bringans, N. Hower, I. Lindau, B.B. Pate, P. Pianetta, L.E. Swartz, R. Tatchyn, Science with Soft X-rays, SPIE Proceeding Series 10 (1984).
3. H. Winick, G. Brown, K. Halbach, and J. Harris, Physics Today, 34 , 50 , May, 1981. and K. Halbach, J. Chin, E. Hoyer, H. Winick, R. Cronin, J. Yang, and Y. Zambre, IEEE Trans. Nucl. Sci. NS28, (1981).
4. G. Brown, K. Halbach, J. Harris, and H. Winick, Nucl. Inst. and Meth., 208, 65, (1983).
5. K. Halbach, Nucl. Inst. and Meth., 187, 109, (1981).
6. T. Cox and B. Youngman, this proceedings.
7. R.D. Bringans et al, to be published.
8. M.H. Hecht, R.D. Bringans, I. Lindau, and R.Z. Bachrach, Nucl. Inst. and Meth., 208, 113, (1983).
9. V. Rehn, AIP Conf. Proc #75. D.T. Attwood and B.L. Hinks eds. p162, (1981).
10. F.C. Brown, R.Z. Bachrach, and N. Lien, Nucl. Inst. and Meth., 152, 73, (1978).
11. F.C. Brown, S.L. Hulbert, and N.C. Lien, 6th Int Conf on VUV Physics (1980), unpublished; S.L. Hulbert, J.P. Stott, F.C. Brown, and N.C. Lien, Nucl. Inst. and Meth., 208, 43, (1983).
12. R.L. Johnson, Proc Int Conf on X-ray and VUV Synchrotron Rad Inst. 1985, Nucl. Inst. and Meth. in press (1986).
13. A. Franks and M. Stedman, Nucl. Inst. and Meth., 172, 249, (1980).
14. H. Petersen, Optics Comm. 40, 402, (1982).
15. F.C. Brown and S.L. Hulbert, Nucl. Inst. and Meth., 222, 42, (1984).
16. V. Rehn, J.L. Stanford, A.D. Baer, V.O. Jones, W.J. Choyke, Appl Optics, 16, 1111, (1977).
17. M.R. Howells, editor, Reflecting Optics for Synchrotron Radiation, SPIE Proceedings 315, (1981).
18. M. Lewis, Proc Int Conf on X-ray and VUV Synchrotron Rad Inst. 1985, Nucl. Inst. and Meth. in press (1986).

19. For information contact: H.Y. Chmait, TRW Space and Technology Group, Optics Dept 01/1141, One Space Park, Redondo Beach, Ca 90278. (213) 536-4278.
20. B. Lai and F. Cerrina, Proc Int Conf on X-ray and VUV Synchrotron Rad Inst. 1985, Nucl. Inst. and Meth. in press (1986).
21. R. Tatchyn and I. Lindau, Nucl. Inst. and Meth., Proc Int Conf on X-ray and VUV Synchrotron Rad Inst. 1985, Nucl. Inst. and Meth. in press (1986).
22. B.B. Pate, to be published
23. J. Cerino, J. Stohr, N. Hower, and R.Z. Bachrach, Nucl. Inst and Meth., **172**, 227, (1980); G.V. Hansson, B. Goldberg and R.Z. Bachrach, Rev. Sci. Instr. **52**, 517, (1981).
24. J. Gailup and R.Z. Bachrach, SSRL Report.

END

DTC

8 — 86